



NAM

IN-PLANE TESTS ON REPLICATED MASONRY WALLS

Physical Testing and Modelling – Masonry Structures

Geert Ravenshorst and Francesco Messali

TU Delft

Date April 2016

Editors Jan van Elk & Dirk Doornhof

General Introduction

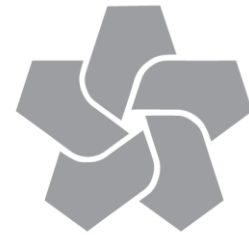
For the modeling of the seismic response of unreinforced masonry buildings, knowledge of the properties of building material is essential. An experimental program to test the properties of the building materials used in the Groningen area was therefore executed. This included measurements of material in existing buildings (Ref. 1) and in laboratories (Ref. 2 and 3).

A previous report (Ref. 4) described experiments for the characterization of replicated masonry wall elements of calcium silicate and clay bricks. The current report describes in-plane cyclic test experiments on large wall units. Both wide and slender walls have been tested. These tests complement the shake test performed on slender and wide wall units in Eucentre, Pavia (Ref. 5).

Test set-up and testing procedures are presented and results discussed. Much attention was given to recording of the failure (crack) pattern in the walls. The results of these experiments, response of wall units, has been used in the calibration for modelling of the seismic response of masonry buildings (Ref. 6, 7 and 8).

References

1. In-situ testing of URM houses (building unit: Loppersum, Zijlvest 25), Eucentre (F. Graziotti, A. Rossi, I. Senaldi, S. Peloso), 5th December 2014.
2. Material Characterisation – Version 1.3, Eucentre, P&P, TU-Delft, TU-Eindhoven, October 2015.
3. Summary report for the characterisation of original Groningen masonry, TU Delft (S. Safari, J. Rots), 18th December 2015.
4. Tests for the characterisation of replicated masonry and wall ties, TU Delft (R. Esposito, F. Messali, J. Rots), 18th April 2016
5. Experimental campaign on cavity walls systems representative of the Groningen building stock (incl. EUC-BUILD1), Eucentre (F. Graziotti, U. Tomassetti, A. Rossi, S. Kallioras, M. Mandirola, E. Cenja, A. Penna, G. Magenes), 16th June 2016.
6. URM Modelling and Analysis Cross Validation – Arup, Eucentre, TU Delft, Reference 229746_032.0_REP127_Rev.0.03 April 2015.
7. Eucentre Shake-table Test of Terraced House Modelling Predictions and Analysis Cross Validation, staff from ARUP, Eucentre (Pavia) and TU Delft, November 2015 [this document also includes; (1) Instruments full-scale test-house Eucentre Laboratory, (2) Protocol for Shaking Table Test on Full Scale Building (Eucentre) V_1, and (3) Selection of Acceleration Time-Series for Shake Table Testing of Groningen Masonry Building at the EUCENTRE, Pavia, all three by staff from Eucentre (Pavia)].
8. Laboratory component testing: Modelling post-test predictions and analysis cross-validation, ARUP, TU Delft and Eucentre (several staff members from all three institutions), 16th February 2016.



NAM

Title	IN-PLANE TESTS ON REPLICATED MASONRY WALLS Physical Testing and Modelling – Masonry Structures		Date	April 2016
			Initiator	NAM
Autor(s)	Geert Ravenshorst and Francesco Messali	Editors	Jan van Elk and Dirk Doornhof	
Organisation	TU Delft	Organisation	NAM	
Place in the Study and Data Acquisition Plan	<p><u>Study Theme:</u> Seismic Response of Buildings (URM)</p> <p><u>Comment:</u> For the modeling of the seismic response of unreinforced masonry buildings, knowledge of the properties of building material is essential. An experimental program to test the properties of the building materials used in the Groningen area was therefore executed. This included measurements of material in existing buildings (Ref. 1) and in laboratories (Ref. 2 and 3). A previous report (Ref. 4) described experiments for the characterization of replicated masonry wall elements of calcium silicate and clay bricks. The current report describes in-plane cyclic test experiments on large wall units. Both wide and slender walls have been tested. These tests complement the shake test performed on slender and wide wall units in Eucentre, Pavia (Ref. 5). Test set-up and testing procedures are presented and results discussed. Much attention was given to recording of the failure (crack) pattern in the walls. The results of these experiments, response of wall units, has been used in the calibration for modelling of the seismic response of masonry buildings (Ref. 6, 7 and 8).</p>			
Directly linked research	<ul style="list-style-type: none"> (1) Building Material properties (2) Shake table tests (3) Fragility curves for building typologies (URM) (4) Risk Assessment 			
Used data	Experiments			
Associated organisation	NAM			
Assurance	TU Delft			

Project number	C31B60
Report number	
Date	April 18, 2016
Version	5
Status	Final

IN-PLANE TESTS ON REPLICATED MASONRY WALLS

Physical Testing and Modelling – Masonry Structures

Client: Nederlandse Aardolie Maatschappij B.V.

Authors Geert Ravenshorst
G.J.P.Ravenshorst@tudelft.nl
Francesco Messali
F.Messali@tudelft.nl

Address Delft University of Technology
Faculty of Civil Engineering and Geosciences
Stevinweg 1, 2628 CN, Delft

Copyright statement

All rights reserved. No part of this publication may be reproduced, stored in a retrieval system of any nature, or transmitted, in any form or by any means, electronic, mechanical, photocopying, recording or otherwise, without the prior written permission of TU Delft.

Liability statement

TU Delft and those who have contributed to this publication did exercise the greatest care in putting together this publication. However, the possibility should not be excluded that it contains errors and imperfections. Any use of this publication and data from it is entirely on the own responsibility of the user. For everybody who has contributed to this publication, TU Delft disclaims any liability for damage that could result from the use of this publication and data from it, unless the damage results from malice or gross negligence on the part of TU Delft and/or those who have contributed to this publication.

Table of Contents

1	Description of test set-up and test specimen.....	4
1.1	General overview.....	4
1.2	Description of the measurement system	5
1.2.1	Specific strategy to measure the net displacement for the short walls (samples TUD_COMP-0a/3)	7
1.2.2	Specific strategy to measure the net displacement for the long walls (samples TUD_COMP-4/6)	8
1.3	Load application for the cantilever test and the double clamped test.	9
1.4	Loading protocol	10
2	Primary results.....	12
3	Crack pattern evolution and remarks for every single tests	17
3.1	TUD_COMP-0a	17
3.2	TUD_COMP-1	19
3.3	TUD_COMP-2.....	21
3.4	TUD_COMP-3.....	23
3.5	TUD_COMP-4.....	25
3.6	TUD_COMP-5.....	28
3.7	TUD_COMP-6.....	31
4	Comparison with values proposed by the codes	36
5	Conclusions	38
	References.....	40

1 Description of test set-up and test specimen

1.1 General overview

The experimental set-up for the in-plane cyclic tests was designed making use of the steel-frame assembling system at the TU Delft in combination with the available anchor points in the strong concrete laboratory floor.

The system consisted of horizontal and vertical actuators. The horizontal actuator had a capacity of 400 kN. For the axial loading, four vertical actuators with a capacity of each 100 kN were used. The vertical loading in the actuators could be differentiated to achieve two different boundary conditions: cantilever (shear span $H_0/H=1.0$) and double clamped situation ($H_0/H=0.5$). The actuator control was managed by software.

The specimen were glued on a bottom steel beam and also a steel beam was glued on top of the masonry. The bottom and top brick layer were glued with "Sikadur 30" to the steel beams to prevent sliding shear failure and tension failure at the steel-masonry contact layer. Failure due to tensile bending stresses or shear failure could therefore occur only in the masonry and not at the steel-masonry contact layer. The bottom steel beam was attached to cross-beams that were connected to the frame that was anchored to the floor, and therefore prevented from uplift. On the top steel beam a load-spreading beam was bolted. The horizontal actuator was attached to this load-spreading beam. The horizontal actuator induced a cyclic shear force on the test specimen. The vertical actuators were loaded in tension and were positioned by a steel frame on the load-spreading beam. This steel-frame was horizontally supported to prevent out-of-plane deformation. The vertical actuators were controlled pairwise, to ensure that the actuator load in each pair was the same. The rotation out-of-plane of the top beam and the load spreading beam was prevented by the frame that introduced the tension force of the vertical actuators (cross section B in Figure 1 and Figure 2).

Two different geometries were evaluated: "short walls" (1.1m long, 2.7m high) and "long walls" (4m long, 2.7m high). With respect to the test set-up for the short walls, on the long walls the vertical actuators were moved outwards to create a larger lever arm; consequently, two extra steel beams were added above the load spreading beam to ensure a uniform spreading of the vertical load on the top of the masonry wall.

The vertical load due to the self-weight of the steel top beam, the load spreading beam and the frames for the vertical actuators is 17 kN for the small specimen and 24 kN for the large specimen. These values were subtracted from the total load to determine the load to be delivered by the vertical actuators.

A scheme of the test set-up employed for the short and the long walls is displayed in Figure 1 and Figure 2, respectively.

A summary of the main features of the tested specimens is reported in Table 1.

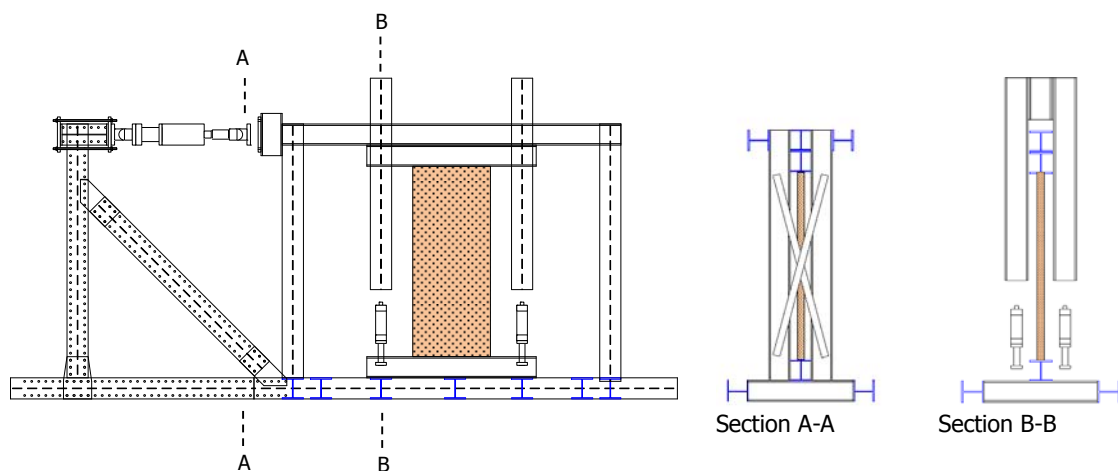


Figure 1. Scheme of the test set-up used for the in-plane tests on short walls.

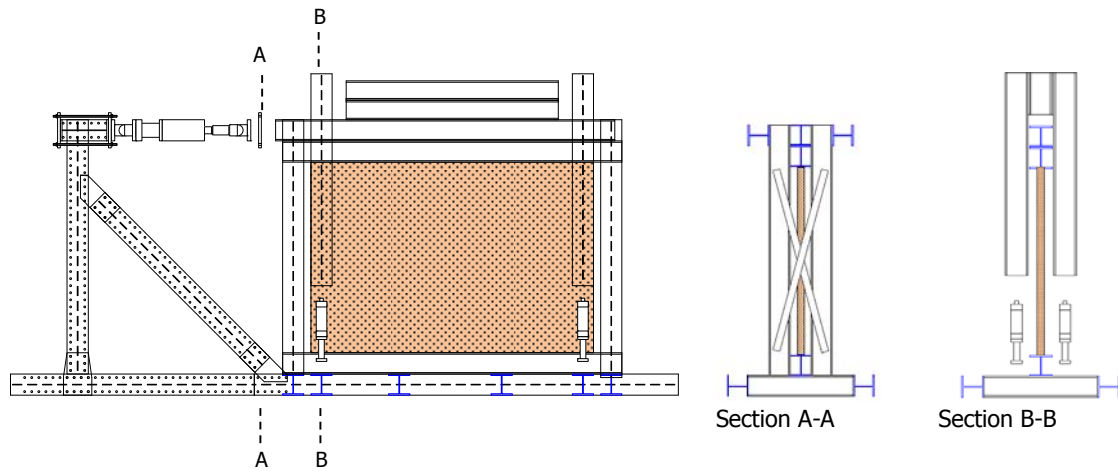


Figure 2. Scheme of the test set-up used for the in-plane tests on long walls.

Table 1. Dimension and features of the test samples.

Name	Dimensions L(m) x H (m) x t (m)	Vertical pressure (MPa)	Shear Span (H ₀ /H)	Test performed at
TUD_COMP-0a	1.1 x 2.76 x 0.102	0.7	0.5	22 June 2015
TUD_COMP-1	1.1 x 2.76 x 0.102	0.7	1	13 July 2015
TUD_COMP-2	1.1 x 2.76 x 0.102	0.5	1	29 June 2015
TUD_COMP-3	1.1 x 2.76 x 0.102	0.4	0.5	13 August 2015
TUD_COMP-4	4.0 x 2.76 x 0.102	0.5	0.5	14 September 2015
TUD_COMP-5	4.0 x 2.76 x 0.102	0.3	0.5	1 October 2015
TUD_COMP-6	4.0 x 2.76 x 0.102	0.5	1	14 October 2015

1.2 Description of the measurement system

The objective of the measurement recordings during the test were:

- to record the global horizontal and vertical deformations;
- to record local deformations and follow the cracking patterns;
- to record the applied forces during the test;
- to produce time-displacement diagrams, time-forces diagrams and force-displacement diagrams.

Figure 3 and Figure 4 give an overview of the measuring points for the in-plane tests on the short specimens (TUD_COMP-0a, TUD_COMP-1, TUD_COMP-2 and TUD_COMP-3), and for the long specimens (TUD_COMP-4, TUD_COMP-5 and TUD_COMP-6), respectively.

In table 2, the intended measurement is described together with the sensor type used and the possible stroke in both directions from the centre position for each measurement point.

The measure points for the photogrammetry (21) will be positioned at bricks all over the specimen on one side of the specimen.

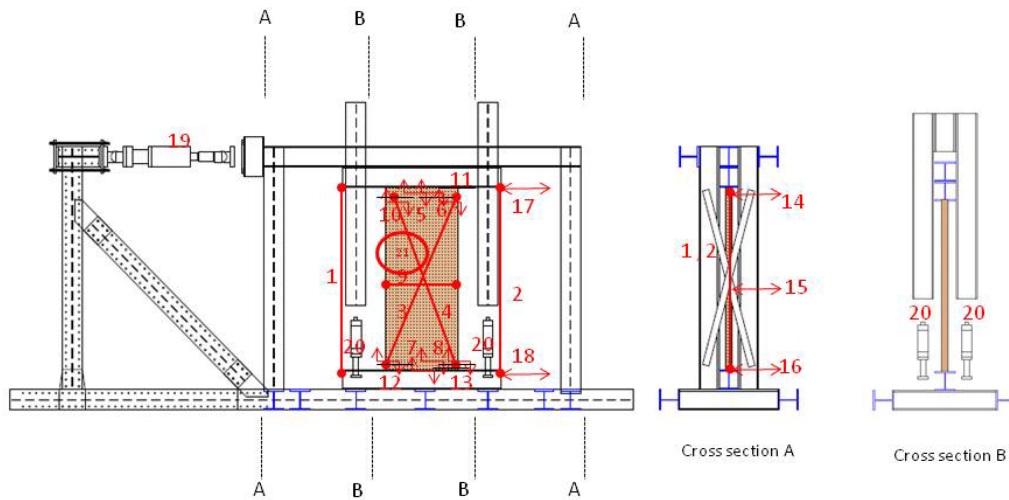


Figure 3. Overview of the measuring points for the short specimens for the in-plane tests at TU Delft.

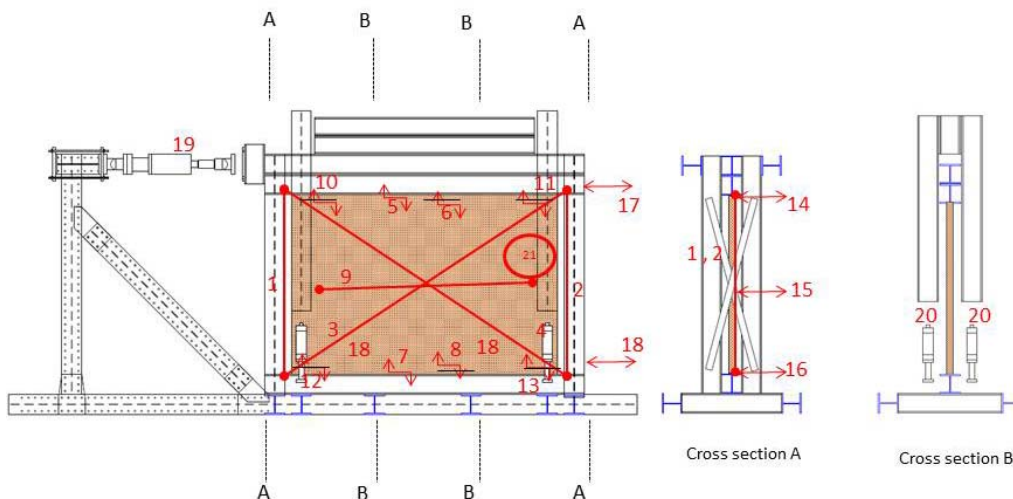


Figure 4. Overview of the measuring points for the long specimens for the in-plane tests at TU Delft.

Table 2. Overview of the measuring points and sensor types for the in-plane tests.

No.	Description	Sensor Type	Stroke (mm)
1	Vertical displacement top beam –bottom beam left (center)	Draw wire	+/-50
2	Vertical displacement top beam –bottom beam right (center)	Draw wire	+/-50
3	Displacement from left bottom on steel beam-right top on steel beam (front)	Draw wire	+/-100
4	Displacement from left top on steel beam-right bottom on steel beam (front)	Draw wire	+/-100
5	Horizontal displacement top steel beam-first top brick layer	Linear potentiometer	+/-10
6	Horizontal displacement first top brick layer -second top brick layer	Linear potentiometer	+/-10

7	Horizontal displacement bottom steel beam-first bottom brick layer	Linear potentiometer	+/-10
8	Horizontal displacement first bottom brick layer -second bottom brick layer	Linear potentiometer	+/-10
9	Horizontal displacement midheight brick layer (front)	Draw wire	+/-50
10	Vertical displacement top left (front)	Linear potentiometer	+/-10
11	Vertical displacement top right (front)	Linear potentiometer	+/-10
12	Vertical displacement bottom left (front)	Linear potentiometer	+/-10
13	Vertical displacement bottom right (front)	Linear potentiometer	+/-10
14	Horizontal displacement out of plane top	Laser	+/-100
15	Horizontal displacement out of plane middle height	Laser	+/-100
16	Horizontal displacement out of plane bottom	Laser	+/-100
17	Horizontal displacement top beam	Draw wire	+/-100
18	Horizontal displacement bottom beam	Draw wire	+/-100
19	Actuator 400 kN – load and displacement	Load cell and HBM LVDT	+/-100
20	Actuator 100 kN (4x)-load and displacement	Load cell and HBM LVDT	+/-20
21	Measure points for photogrammetry	stickers	

In this report the results are presented in graphs showing the measured shear force plotted against the measured net displacement (the horizontal deformation of the top of the masonry wall relative to the bottom of the masonry wall).

A counterweight was applied in order to compensate the weight of the horizontal actuator (19 in Table 2 and Figure 4) on the load cell and an eccentric weight of steel plates on the loadspreading beam (W_E) in figure xxx.

For specimens TUD_COMP-0a and TUD_COMP-2 the eccentric load W_E was not compensated by the counterweight; consequently, the eccentric load (P_e) determined some asymmetries in the wall responses, that has been taken into account in the presented tabellised results and graphs by compensating the measured force with an imposed torque ($M = W_E \cdot e$) applied at the top of the walls.

1.2.1 Specific strategy to measure the net displacement for the short walls (samples TUD_COMP-0a/3)

The deformability of the frame determined a difference between the displacement imposed to the horizontal actuator (described in section 1.4) and the actual net displacement applied to the top of the wall.

Specifically, the cross beams (1, in Figure 5) which supported the beam (2) below the wall were not directly positioned at the floor but spanned between lengthwise positioned beams that were anchored to the laboratory floor. Therefore, the crossbeams (1) could deform elastically vertically both upwards and downwards; consequently, the beam (2) at the base of the wall could rotate. This will give an additional horizontal deflection at the top for H1.

From test TUD_COMP-1, the introduction of additional transducers allowed to assess the size of this difference. Specifically, as shown in Figure 5, four vertical transducers (OS1-4) recorded the absolute vertical displacements of the bottom beam which support the wall (accordingly, the rigid rotation of the

beam could be computed). A fifth transducer (OS5) measured the relative displacement of the top of the wall with respect to the top of a steel column (3).

The net deflection of the wall was obtained according to the 2 following procedures for cross-validation.

- a. By calculation: subtracting the horizontal displacement of beam 2 (measured by device H2) and the horizontal displacement at the top of the wall determined by the rigid rotation of beam 2 to the "gross" displacement (recorded by device H1).
- b. By direct reading of transducer OS5. Indeed, column 3 was affected by the same rigid rotation of the wall, since it was bolted at the base to beam 2.

Besides, the absence of any sliding between the wall and the top/bottom beams was assessed.

The calculated net deflection obtained by the methods a and b showed good correlation. The net deflections are presented are primarily obtained by method b.

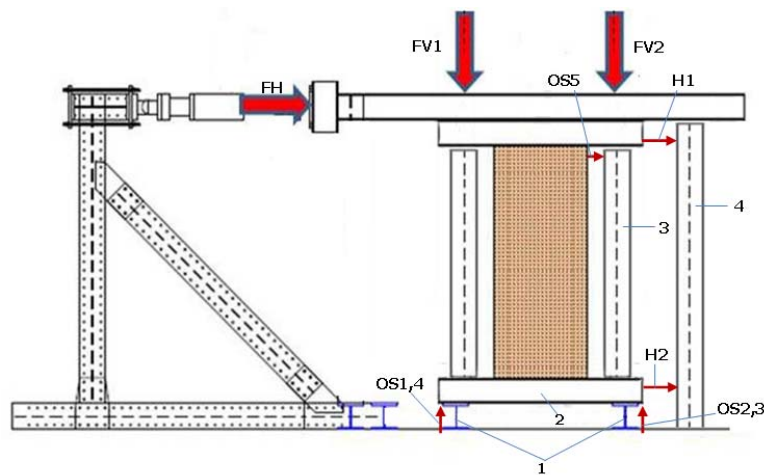


Figure 5. Transducers employed to measure the net deflection of the tested walls.

1.2.2 Specific strategy to measure the net displacement for the long walls (samples TUD_COMP-4/6)

In case of long walls, given the high stiffness of the specimens, a specific accurate evaluation of the effective net displacements of the top with respect to the bottom of the wall has been taken into account. Hence, additionally to the system described in the previous section, an additional diagonal sensor, from the bottom-middle to the top-right corner of the wall, was placed (as described in Figure 6).

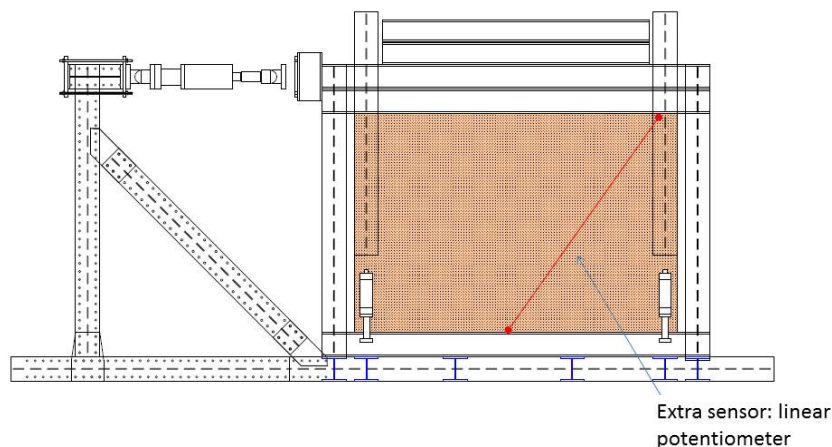


Figure 6. Position of the extra diagonal sensor in long walls (specimen TUD_COMP-4/6).

The reading of the diagonal elongation (provided by this additional sensor), combined with the vertical extension (measured by sensors 1 and 2 in Table 2 and Figure 4), provide a direct measure of the deformation of the wall, and consequently of the net displacement. For the long walls the presented net deflections are obtained by this method.

1.3 Load application for the cantilever test and the double clamped test.

Two mechanical schemes with different boundary conditions were applied, either as a cantilever, or as a double clamped wall. The mechanical scheme for the cantilever tests (shear span $H_0/H=1$) is given in Figure 7a; the mechanical scheme for the double clamped tests (shear span $H_0/H=0.5$) is given in Figure 7b. The forces F_S and F_D were applied by the vertical actuators. W_H is the weight of the horizontal actuator. W_T is the weight of the top steel beam, the load spreading beam and the frame for the vertical actuators. i is the length between the pairs of vertical actuators, l_t is the length of the load spreading beam, h_m is the height of the masonry wall and h_o is the distance between the system line of the horizontal force F_H . The total load P is the required vertical compression force.

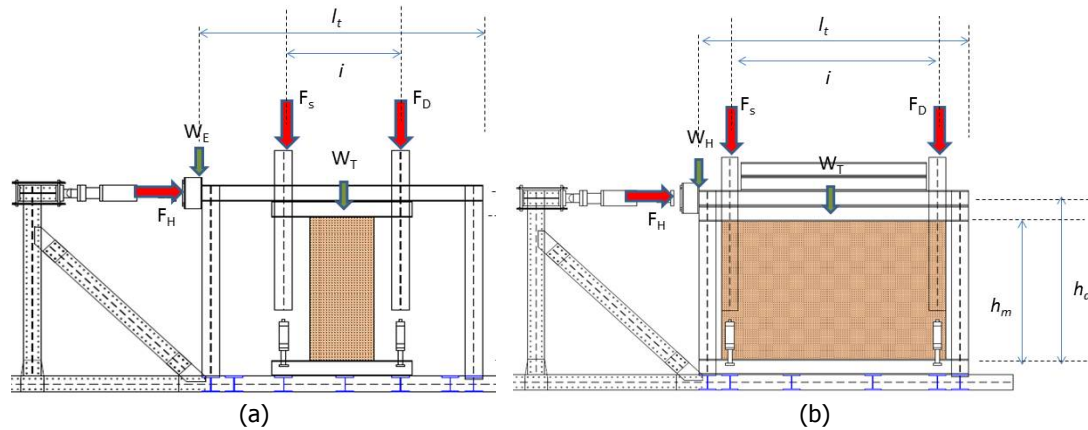


Figure 7. Load application on the short (a) and long (b) walls, respectively.

Determination of the vertical loads for the cantilever test.

The following equations were employed to control the applied vertical forces:

$$\begin{cases} F_D + F_S + W_E + W_T = P \\ F_D \frac{i}{2} = F_S \frac{i}{2} + \frac{W_E l_T}{2} \end{cases} \quad (1)$$

The forces to be delivered by the vertical actuators are then calculated by:

$$\begin{cases} F_S = \frac{P}{2} - \frac{W_T}{2} - \frac{W_E}{2} \left(1 + \frac{l_T}{i}\right) \\ F_D = \frac{P}{2} - \frac{W_T}{2} - \frac{W_E}{2} \left(1 - \frac{l_T}{i}\right) \end{cases} \quad (2)$$

The force F_S and F_D remained constant during the test, and were not related to the horizontal force F_H .

Determination of the vertical loads for the double clamped test.

For the double clamped test a "kinematic" criterion is applied. The following equations are fulfilled during the test:

$$\begin{cases} F_D + F_S + W_E + W_T = P \\ u_D = u_S \end{cases} \quad (3)$$

Where u_D and u_S are the vertical displacements of the vertical pairwise actuators (these requirement were dynamically updated during the test).

The force F_S and F_D are dynamically updated according to the "kinematic" criterion, and are therefore related to the horizontal force F_H . In Table 3, the starting values for F_S and F_D at the start of the test are given.

Table 3 gives the positions and values of the applied forces.

Table 3. Position and value of applied forces.

Name	i (m)	l_T (m)	h_m (m)	h_θ (m)	F_D (kN)	F_S (kN)	W_T (kN)	W_E (kN)
TUD_COMP-0a	1.9	4.8	2.76	3.15	30.0 ¹	30.0 ¹	17	1.7
TUD_COMP-1	1.9	4.8	2.76	3.21	30.0	30.0	17	0
TUD_COMP-2	1.9	4.8	2.76	3.21	19.0	19.0	17	1.7
TUD_COMP-3	1.9	4.8	2.76	3.21	13.5 ¹	13.5 ¹	17	0
TUD_COMP-4	3.7	4.8	2.76	3.21	90.0 ¹	90.0 ¹	24	0
TUD_COMP-5	3.7	4.8	2.76	3.21	49.2 ¹	49.2 ¹	24	0
TUD_COMP-6	3.7	4.8	2.76	3.21	90.0	90.0	24	0

¹ Starting values at the beginning of the test.

1.4 Loading protocol

The loading protocol was performed as follows:

For the cantilever tests:

- The vertical loads are applied. They remain constant during the test;
- The horizontal actuator force F_H is applied. The first cycle is applied in force control. The force is then raised up to the 25% of the maximum expected force;
- The horizontal force $F_{H,25\%}$ is applied three times in both directions (a single cycle is defined as three times the same applied load or deformation in both directions);
- After the first cycle, the test is performed in displacement control;
- The 2nd to 4th cycle are multiplications of the displacement in the first cycle;
- From the 5th cycle the deformation determine a 0.050% drift, adding 0.025% each cycle, and adding with increasing percentage.

For the double clamped tests:

- The vertical loads are applied. They remain constant during the test;
- The horizontal actuator force F_H is applied. The vertical loads are adjusted according to the requirements listed in section 1.3. The first cycle is applied in force control. The force is raised up to the 25% of the maximum expected force;
- The horizontal force $F_{H,25\%}$ is applied three times in both directions (a single cycle is defined as three times the same applied load or deformation in both directions);
- After the first cycle, the test is performed in displacement control;
- The 2nd to 4th cycle are multiplications of the displacement in the first cycle;

- From the 5th cycle the deformation determine a 0.050% drift, adding 0.025% each cycle, and adding with increasing percentage.

The increasing lateral displacements are obtained by imposing and controlling the displacements of the horizontal actuator (19 in Table 2 and Figure 4); the original loading history is symmetric for positive and negative displacements and follows a regular scheme for every test. However, as introduced in section 1.2.1, the net horizontal displacements presented in section 2 and 3 are measured directly on the samples, in order to remove every additional deformation of the set-up steel frame. Thus, given the elastic deformations of the frame (more details are provided in section 1.2.1), small differences between positive and negative measured displacements, as well as between the different tests, are detected.

2 Primary results

The following results are considered as primary:

- The initial elastic stiffness of the wall (K_{in}), measured as the secant stiffness between the extreme displacements of the first cycle;
- The shear strength of the wall (V^+ , V^- for positive and negative displacements, respectively);
- The prevailing failure mode.

The primary results recorded after each test are reported in Table 4.

σ_v is the uniform and constant vertical pressure applied to the top of the wall, and calculated according to the following equation:

$$\sigma_v = P/(Lt) \quad (4)$$

where P is the applied vertical compression force, L and t are the depth and the thickness of the wall, respectively.

The shear force (V) is evaluated as the force transmitted by the horizontal actuator and measured by the corresponding load cell (19 in Table 2 and Figure 4).

The net horizontal displacement (δ) represent the difference between the absolute displacements of the top of and the bottom of the wall, respectively (Figure 8). Therefore, it is calculated according to the methods given in section 1.2.1 and 1.2.2

The corresponding net drift of the wall is finally evaluated as the ratio between the measured net horizontal displacement (δ) and the wall height (H), as defined in the following equation:

$$d_r = \delta/H \quad (5)$$

Table 4 reports also the final drift ($d_{r,f}$) in percentages ($=d_r \cdot 100$), that is the drift at which each test was stopped; it should not be confused with the ultimate possible drift of the wall, that is the capacity of the wall in terms of displacements.

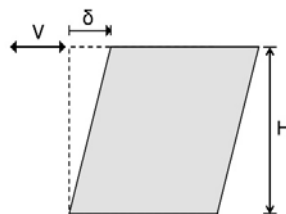


Figure 8. Schematic representation of the deformed wall: identification of the shear force (V), and of the net horizontal displacement (δ).

Besides, the shear force vs the measured horizontal net displacement of the wall is plotted in Figure 9 and Figure 10 for each test performed on short and long walls, respectively. Both the original cyclic curves (a) and the corresponding backbone (b) curves are plotted. The backbone curves are obtained by connecting the shear loads at the extreme displacements of each cycle.

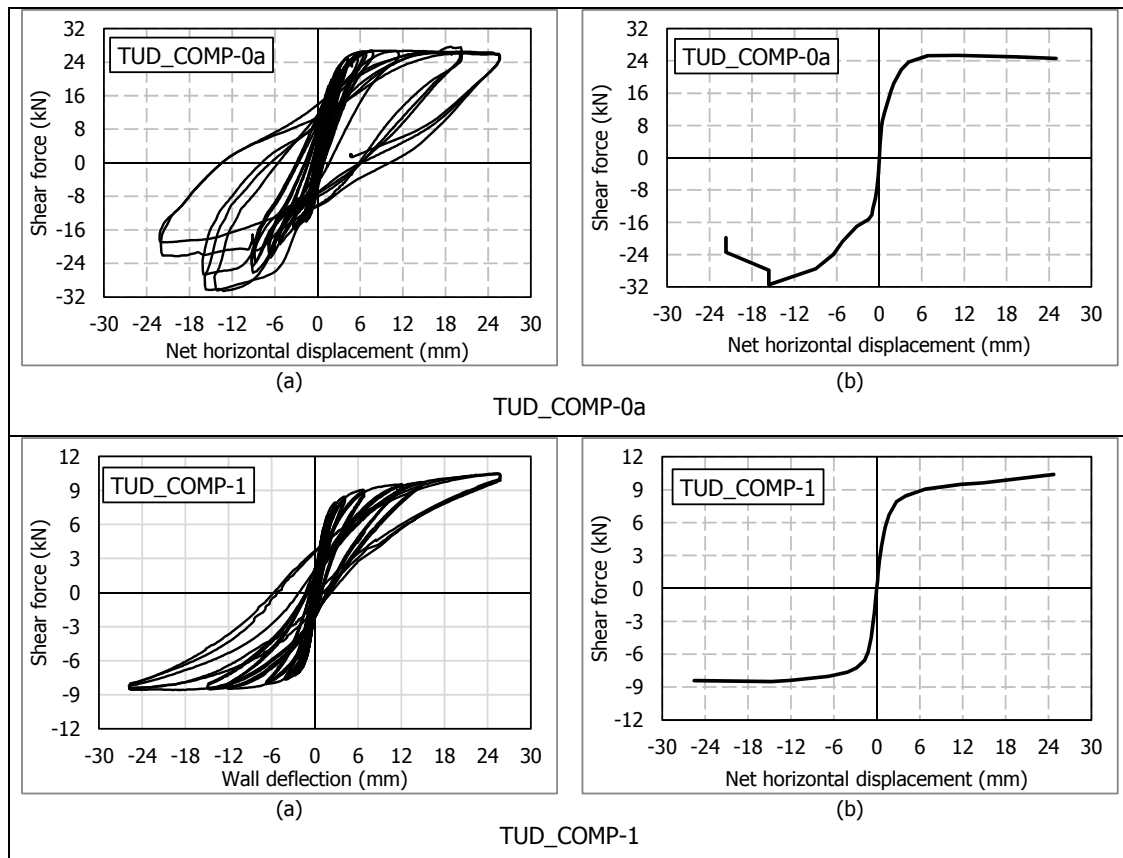
Figure 11 and Figure 12 show a comparison between the backbone curves of the short and long walls, respectively.

It should be remarked that the final drift listed in Table 4 and showed in Figure 11 and Figure 12 are in most cases determined by limitations in the set-up (as detailed explained in section 3), rather than by the effective failure of the specimens.

Table 4. Primary results from the performed in-plane tests.

Specimen	BC	σ_v	K_{in}	V^+	V^-	$d_{r,f}$	Prevailing failure mode
		(MPa)	(kN/mm)	(kN)	(kN)	(%)	
TUD_COMP-0a	DC	0.7	25.8	27.7	-30.6	0.9	Combined: - Flexure; - Toe crushing; - Sliding.
TUD_COMP-1	C	0.7	7.2	9.94	-9.11	0.9	Combined: - Flexure; - Toe crushing; - Sliding.
TUD_COMP-2	C	0.5	7.7	9.40	-9.57	1.6	Combined: - Flexure; - Sliding.
TUD_COMP-3	DC	0.4	22.4	15.0	-14.2	1.3	Combined: - Flexure; - Toe crushing; - Sliding.
TUD_COMP-4	DC	0.5	223	119	-123	0.2	Shear diagonal cracks along joints.
TUD_COMP-5	DC	0.3	288	102	-103	0.45	Sliding along the bottom mortar joint.
TUD_COMP-6	C	0.5	125	110	-109	0.55	Shear diagonal cracks along joints and toe crushing.

Where BC = boundary conditions; σ_v = vertical pressure; K_{in} = initial stiffness (measured as the secant stiffness between the extreme displacements of each cycle); V^+ , V^- = shear strength for positive and negative displacements, respectively; $d_{r,f}$ = final drift (drift at which the test was stopped); DC = double clamped wall; C = cantilever wall.



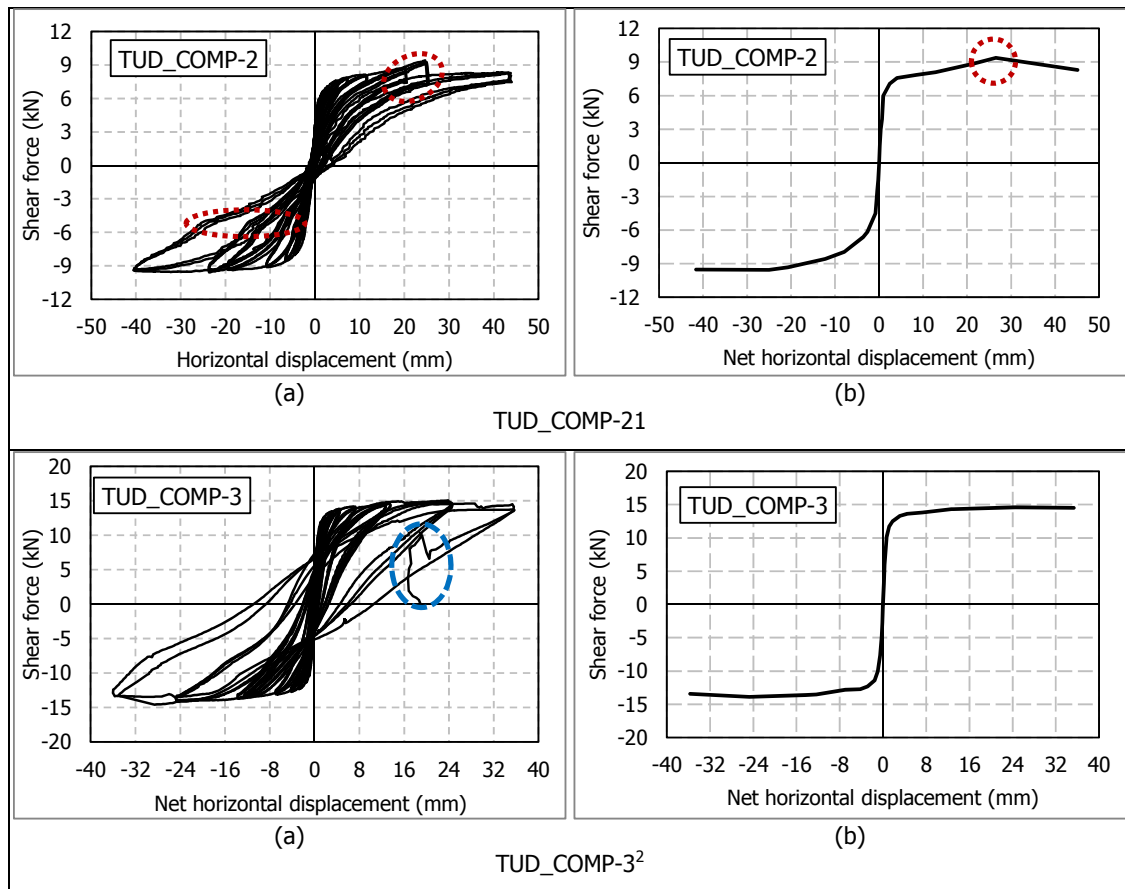


Figure 9. Shear force vs Measured net displacement of the wall for the short walls (TUD_COMP-0a, TUD_COMP-1, TUD_COMP-2 and TUD_COMP-3). Both total (a) and backbone (b) curves are plotted.

¹ The red circle locates some values of forces which cannot be considered reliable, since alterations in the single vertical forces applied by the actuators were measured (despite the total vertical force remained constant throughout the whole test). Further information can be found in section 3.3.

² The end test (in the blue circle) was determined by the instability of the loading system, not by a failure of the wall.

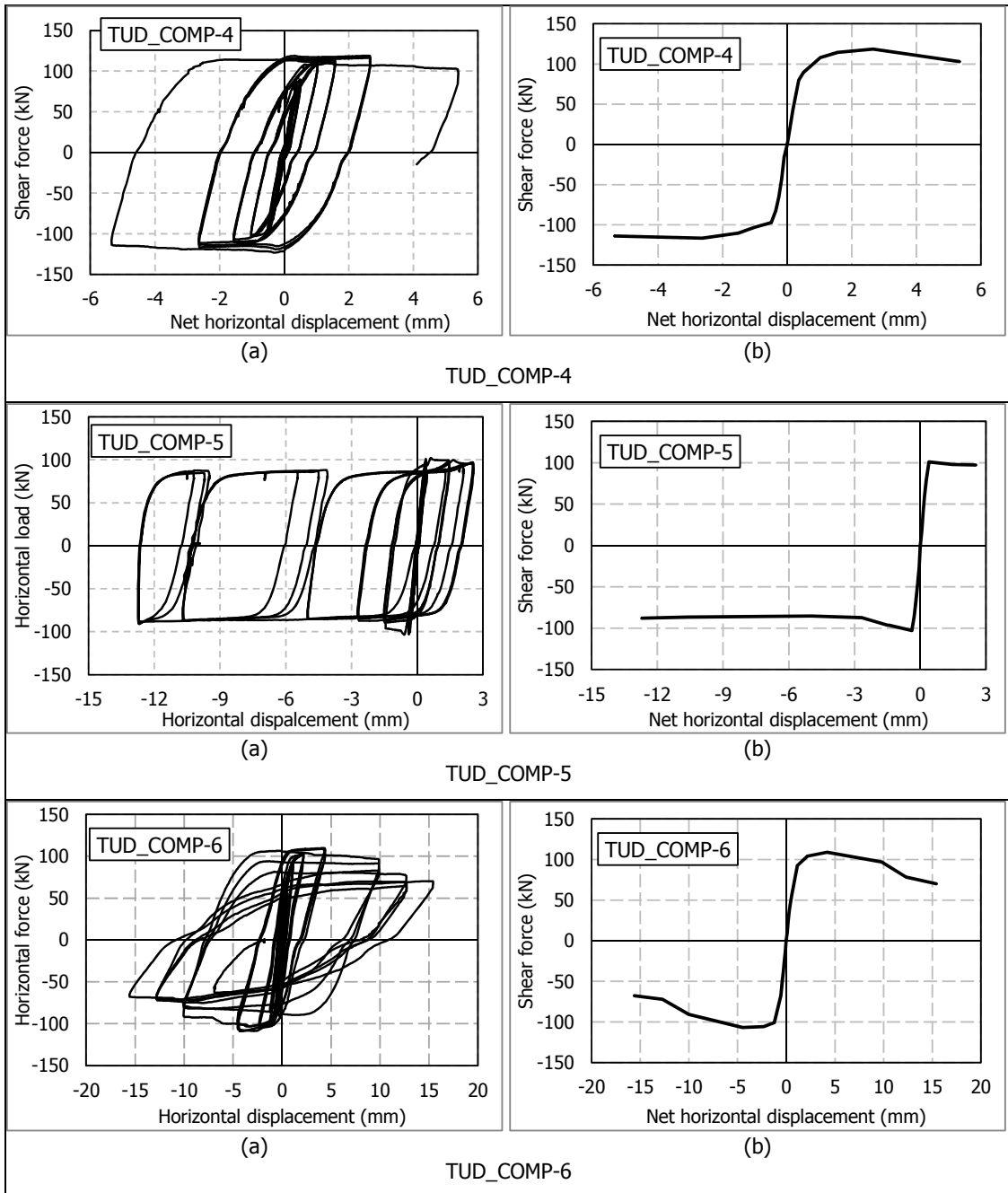


Figure 10. Shear force vs Measured horizontal net displacement of the wall for the long walls (TUD_COMP-4, TUD_COMP-5, and TUD_COMP-6). Both total (a) and backbone (b) curves are plotted.

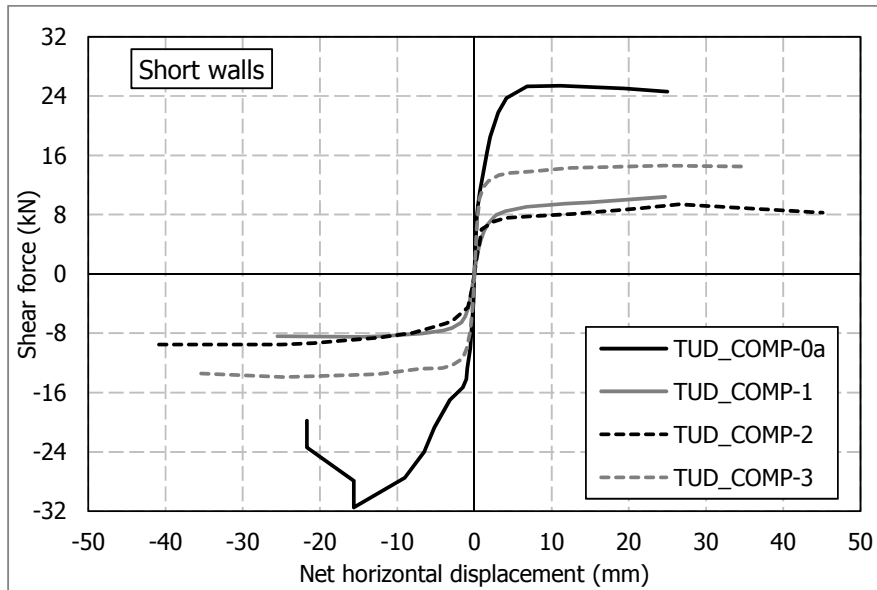


Figure 11. Comparison between the backbone curves of the Shear force vs Measured horizontal net displacement of the wall, for short walls (TUD_COMP-0a, TUD_COMP-1, TUD_COMP-2 and TUD_COMP-3).

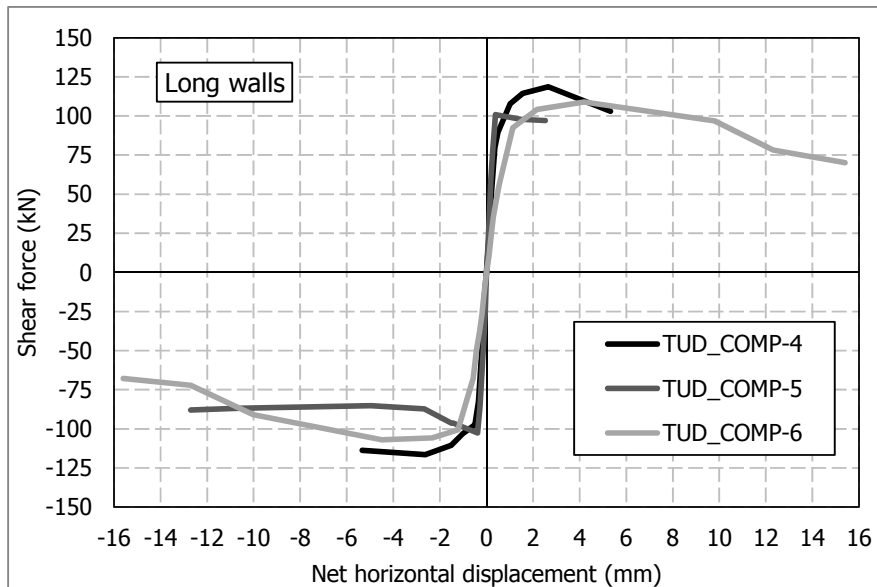


Figure 12. Comparison between the backbone curves of the Shear force vs Measured horizontal net displacement of the wall, for the long walls (TUD_COMP-4, TUD_COMP-5, and TUD_COMP-6).

3 Crack pattern evolution and remarks for every single tests

3.1 TUD_COMP-0a

The recorded net drifts of the wall measured at the positive and negative extremes of each cycle are listed in Table 5.

Table 5. Adopted loading scheme for sample TUD_COMP-0a.

Cycle	Measured net drift (%)		Measured net amplitude (mm)	
	Positive displacements	Negative displacements	Positive displacements	Negative displacements
1	0,004	-0,005	0,11	-0,13
2	0,008	-0,009	0,23	-0,26
3	0,012	-0,014	0,33	-0,39
4	0,016	-0,019	0,43	-0,53
5	0,029	-0,035	0,81	-0,97
6	0,063	-0,041	1,72	-1,14
7	0,077	-0,057	2,12	-1,59
8	0,114	-0,120	3,13	-3,3
9	0,160	-0,194	4,41	-5,33
10	0,251	-0,248	6,91	-6,82
11	0,419	-0,336	11,51	-9,23
12	0,741	-0,336	20,37	-9,23
13	0,936	-0,804	25,75	-22,12

The first three cycles of the test show an elastic behaviour of the specimen; however, a gradual reduction of the initial stiffness occurred at very low drifts, starting from cycle 2 (0.01% drift).

First cracks appear in the mortar bed-joint at the top right corner for positive displacements during cycle 4, as depicted in Figure 13a. From cycle 10, diagonal cracks close to corners develop gradually; a combination of flexure (Figure 13b) and sliding (Figure 13c) is observed. Finally, from cycle 12 splitting of bricks, given by compressive failure, is also observed (Figure 13d).

The crack pattern at end stage is shown in Figure 14. The failure mode combines flexure, sliding and crushing: flexure determined the peak resistance of the specimen, whereas toe crushing causes the eventual reduction of resistance.



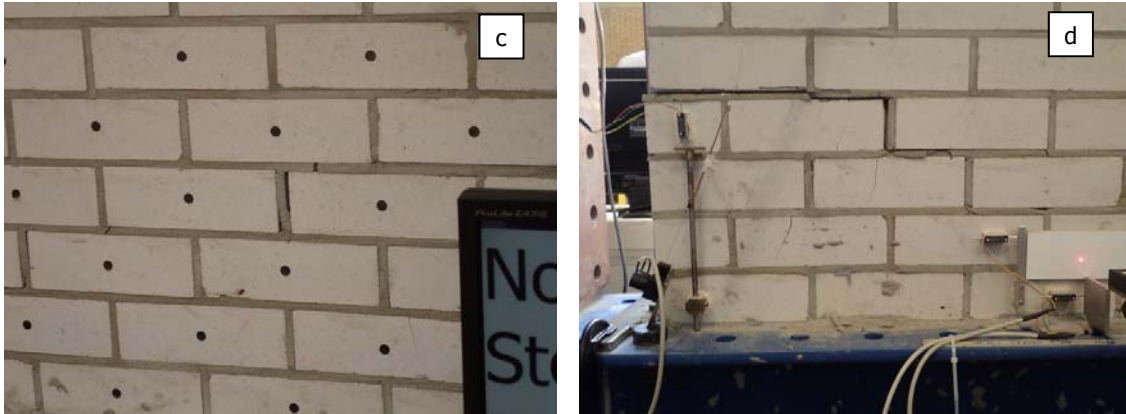


Figure 13. Crack pattern evolution for specimen TUD_COMP-0a: first bed-joint crack (a) - picture taken from the back of the wall; initiation of the diagonal cracks (b); sliding associated to the diagonal cracks (c); initiation of the toe crushing (d).



Figure 14. TUD_COMP-0a: Crack pattern at end stage; general overview (a); detail of the bottom part of the wall (b) and of the toe crushing (c).

During cycle 12, the bolts of the set-up frame were tightened, since some small relative motions were observed; as a probable consequence a reduced stiffness was measured for negative displacements comprised between -2 mm and -9 mm during the previous cycles (cycles 8 to 11), as shown in Figure 15.

The specimen showed also asymmetric general mechanical behaviour (different peak resistance and softening behaviour). This can be explained by the fact that the cracks at the left bottom and top right occurred at a different height than at the right bottom and top left.

The test was stopped after that a large reduction of resistance for negative imposed displacements was measured (-35% with respect to the peak resistance), because the integrity of the wall could have been compromised for larger imposed drifts. Specifically, significant damage of top-right and left-bottom corners, for the splitting/crushing of the toes, was detected.

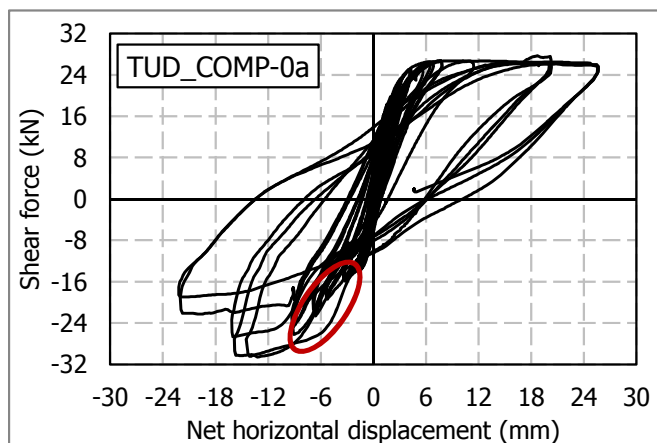


Figure 15. TUD_COMP-0a: change of stiffness before and after tightening the bolts in cycle 12.

3.2 TUD_COMP-1

The recorded net drifts of the wall measured at the positive and negative extremes of each cycle are listed in Table 6.

Table 6. Adopted loading scheme for sample TUD_COMP-1.

Cycle	Measured net drift (%)		Measured net amplitude (mm)	
	Positive displacements	Negative displacements	Positive displacements	Negative displacements
1	0,003	-0,003	0,09	-0,09
2	0,005	-0,007	0,15	-0,19
3	0,013	-0,013	0,35	-0,37
4	0,019	-0,020	0,53	-0,55
5	0,027	-0,028	0,75	-0,76
6	0,043	-0,044	1,20	-1,21
7	0,061	-0,062	1,70	-1,70
8	0,104	-0,104	2,86	-2,88
9	0,150	-0,150	4,13	-4,15
10	0,245	-0,245	6,77	-6,77
11	0,441	-0,442	12,2	-12,2
12	0,522	-0,539	14,4	-14,9
13	0,932	-0,936	25,7	-25,8

The first five cycles show an elastic behaviour of the specimen; however, a gradual reduction of the initial stiffness occurred after cycle 2 (-10% at 0,15‰ drift). First cracks appeared at the bottom corners during cycle 6 ($\pm 0,4\%$ drift), as shown in Figure 16.

During cycle 12 ($\pm 4\%$ drift), new flexural cracks opened, starting from the 6th (positive drifts) or 7th (negative drifts) mortar bed joints; the cracks developed along the mortar joint for approximately the half of the length of the wall, and then was diagonal oriented pointing to the opposite bottom corner of the wall

(Figure 17a,b). At end stage, crushing of the toes and sliding along the flexural cracks could also be observed (Figure 17c,d). Therefore, the failure mode was mainly governed by flexure, but shear sliding contributed to the damage of the specimen. The specimen showed symmetric mechanical behaviour. The test was stopped at a net drift of 1%, after that the maximum allowable extension of the vertical actuators (40 mm) was reached; indeed, the rocking behaviour of the wall determines large vertical displacements of the side of the wall, in correspondence to the position of the actuators.

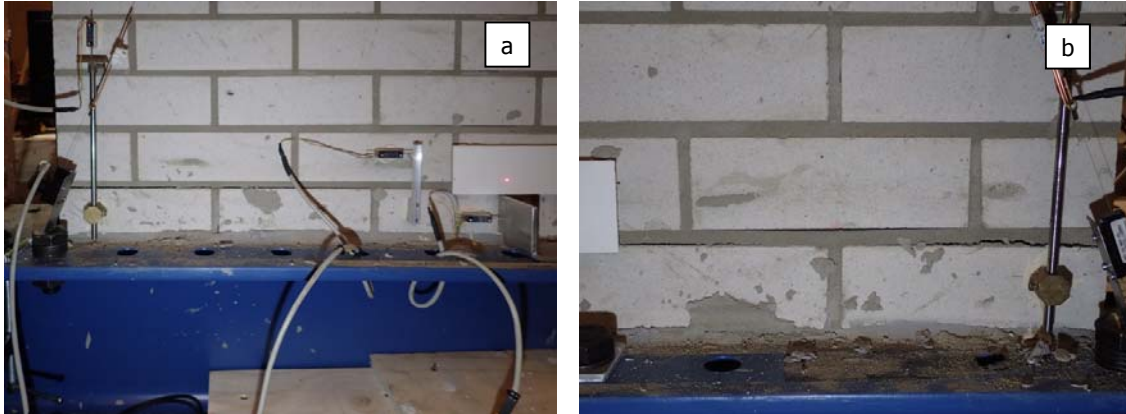


Figure 16. TUD_COMP-1: Rocking cracks at the base of the wall: details of the left (a) and right (b) toes.

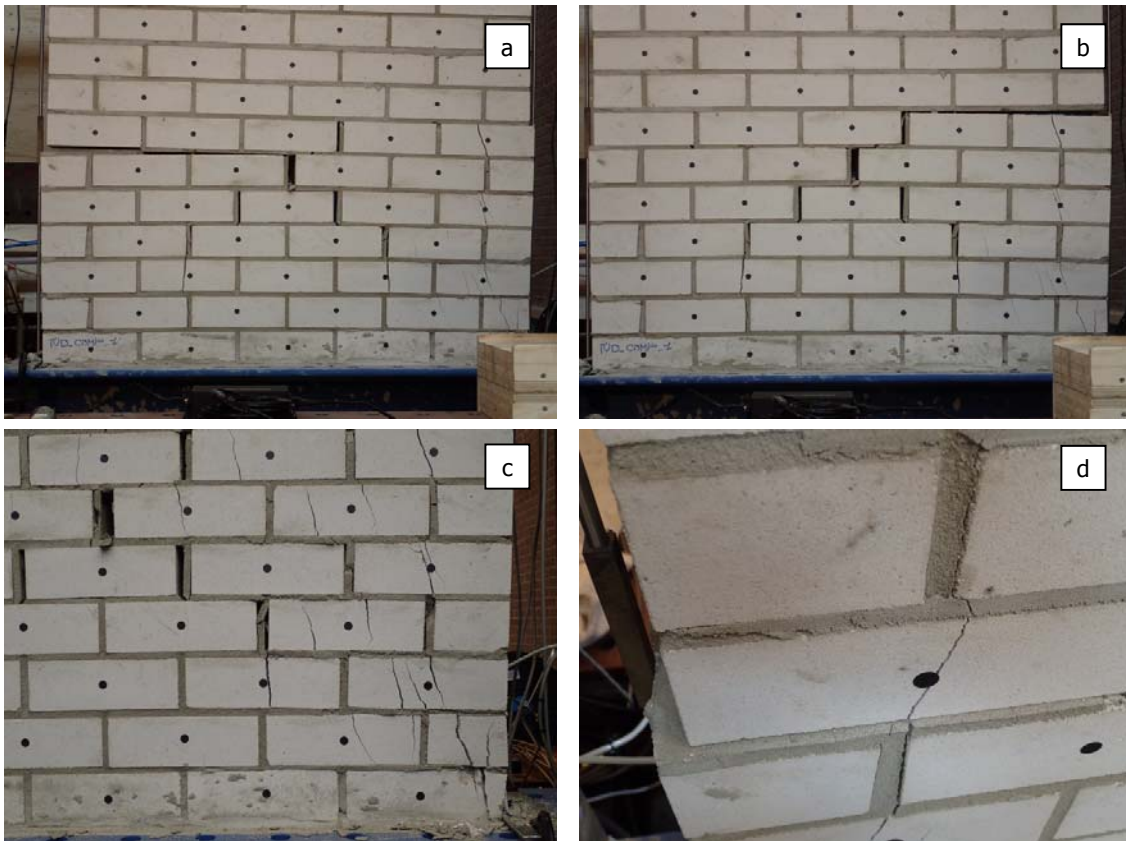


Figure 17. TUD_COMP-1: Crack pattern at end stage for positive (a) and negative (b) drifts; details of the toe crushing (c) and sliding (d) at end stage.

3.3 TUD_COMP-2

The recorded net drifts of the wall measured at the positive and negative extremes of each cycle are listed in Table 7.

Table 7. Adopted loading scheme for sample TUD_COMP-2.

Cycle	Measured net drift (%)		Measured net amplitude (mm)	
	Positive displacements	Negative displacements	Positive displacements	Negative displacements
1	0,007	-0,007	0,19	-0,20
2	0,015	-0,015	0,41	-0,41
3	0,023	-0,022	0,64	-0,61
4	0,034	-0,031	0,94	-0,85
5	0,079	-0,063	2,17	-1,72
6	0,117	-0,089	3,21	-2,44
7	0,272	-0,233	7,48	-6,40
8	0,432	-0,387	11,88	-10,64
9	0,754	-0,702	20,74	-19,30
10	0,934	-0,856	25,68	-23,53
11	1,607	-1,467	44,19	-40,34

The first four cycles showed an elastic behaviour; a gradual reduction of the initial stiffness occurred at very low drifts, starting from cycle 2 (0.015% drift). The first cracks appear at the bottom left corner for negative displacements during Cycle 5 ($\pm 0.7\%$ drift, Figure 18a); then, a crack pattern evolution similar to that of specimen TUD_COMP-1 occurs also for specimen TUD_COMP-2.

During cycle 8 ($\pm 4\%$ drift), new flexural cracks opened (Figure 18b), starting from the 5th (positive drifts) or 6th (negative drifts) mortar bed joints; the cracks developed along the mortar joints partially horizontally and partially diagonally oriented pointing to the opposite bottom corner of the wall. At end stage, crushing of the toes and sliding along the flexural cracks could also be observed (Figure 18c,d). Therefore, the failure mode was mainly governed by flexure, but shear sliding contributed to the damage of the specimen.

The crack pattern at end stage is shown in Figure 19.

Similar to sample TUD_COMP-1, the test was stopped at a net drift of 1,6% after that the maximum allowable extension of the vertical actuators (40 mm) was reached.

The values of the shear force at the positive extreme of cycles 9 and 10 and during the unloading phase of cycle 12 are affected by the bending of the load cell, and cannot be considered reliable. Specifically, Figure 20 shows that, despite the compressive vertical load imposed at the top of the wall remained constant throughout the whole test, differences between the forces applied by the single vertical actuators can be detected; this fact might be associated to an out-of-plane rotation of the top beam that induced a torsion of the load cell (and consequently the aforementioned inaccuracy in the horizontal force measurements).



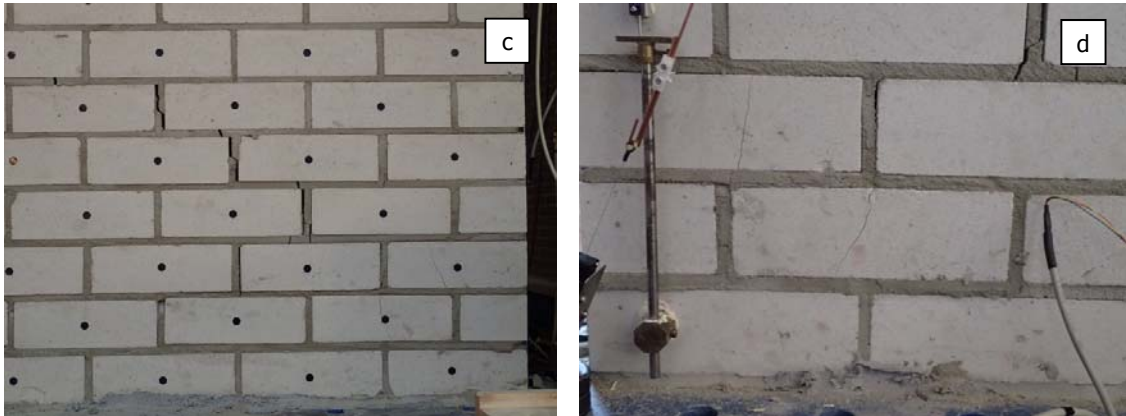


Figure 18. Crack pattern evolution for TUD_COMP-2: first bed-joint crack (a); initiation of the diagonal cracks (b); sliding associated to the diagonal cracks (c); final toe crushing (d).

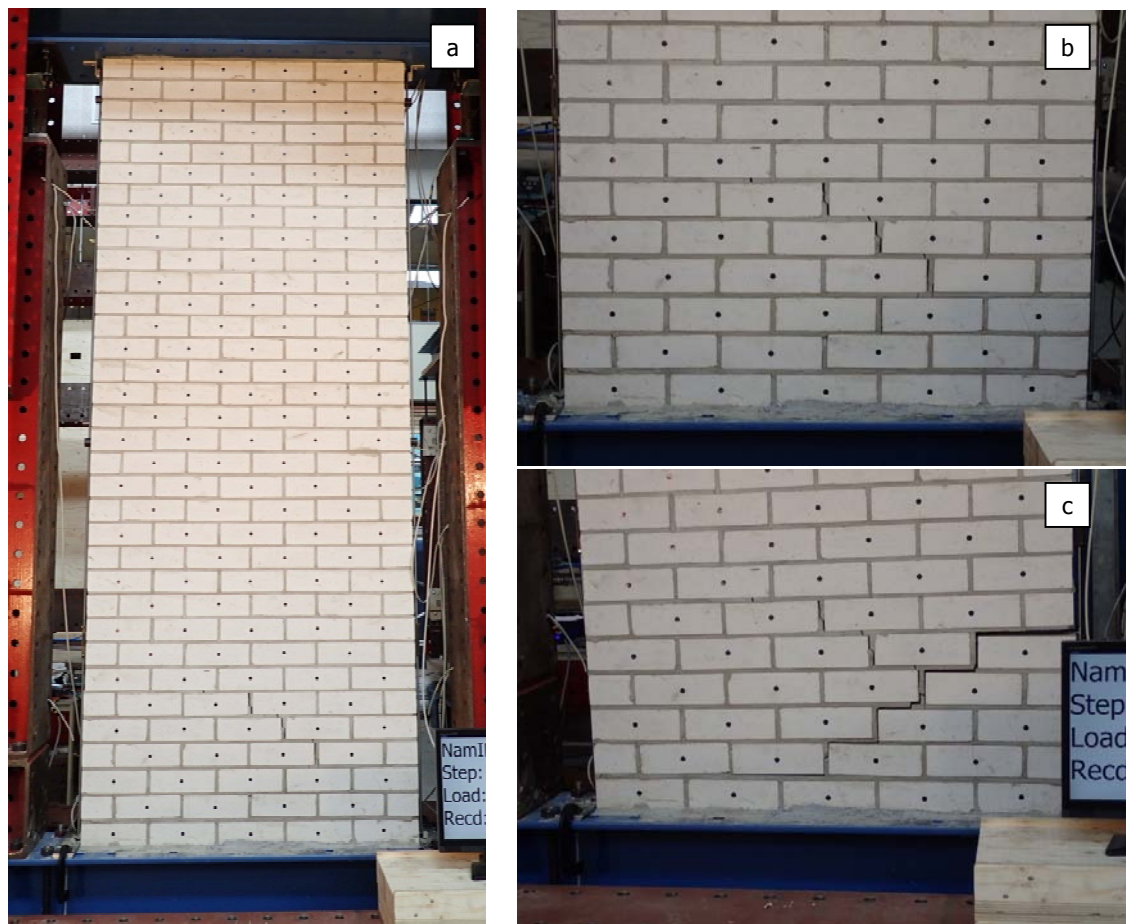


Figure 19. TUD_COMP-2: Crack pattern at end stage; general overview (a); detail of the bottom part of the wall for positive (b) and negative top displacement (c).

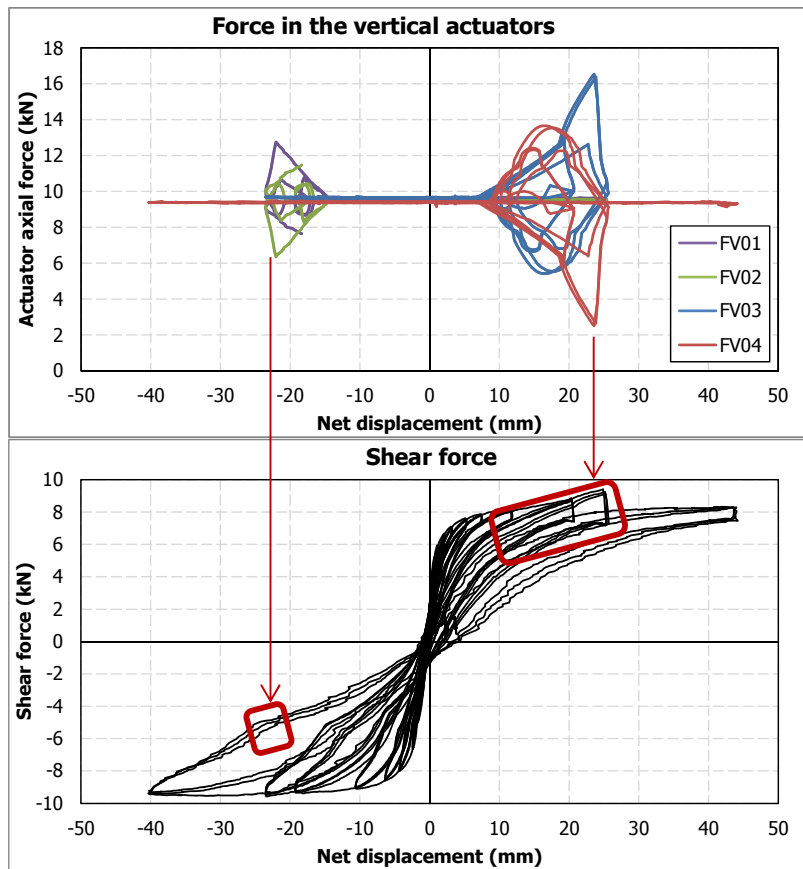


Figure 20. Aberrations of the vertical forces during the test and influence on the wall response.

3.4 TUD_COMP-3

The recorded net drifts of the wall measured at the positive and negative extremes of each cycle are listed in Table 8Table 9.

Table 8. Adopted loading scheme for sample TUD_COMP-3.

Cycle	Measured net drift (%)		Measured net amplitude (mm)	
	Positive displacements	Negative displacements	Positive displacements	Negative displacements
1	0,005	-0,004	0,15	-0,12
2	0,010	-0,009	0,28	-0,24
3	0,024	-0,019	0,67	-0,52
4	0,042	-0,036	1,16	-1
5	0,065	-0,057	1,79	-1,58
6	0,113	-0,103	3,13	-2,85
7	0,163	-0,151	4,51	-4,18
8	0,263	-0,247	7,25	-6,83
9	0,458	-0,455	12,64	-12,57
10	0,488	-0,497	13,48	-13,72
11	0,891	-0,896	24,59	-24,72
12	1,292	-1,304	35,67	-36

The test on specimen TUD_COMP-3 was performed in two phases: first a vertical pressure of 0.3 MPa was applied and the specimen was tested in the elastic phase only; at a later stage, the vertical pressure was raised to 0.4 MPa and the specimen tested to failure. The reason to stop the test TUD_COMP-3a was that the following: The double clamped system ensures the top beam to remain parallel with the bottom beam during the test. To achieve this the total vertical force remains constant, but the division between the two vertical loads changes. Indeed, during the first phase of the test, one of the two forces in the actuators became negative, meaning that the actuators had to push instead of pull (even if this does not mean that the masonry wall was pulled, because of the self-weight of the top beams). Since the actuators can only give a small pushing force, to avoid instability in the test set-up the test had to be stopped and a larger initial tensile force had to be applied to the actuators. This resulted in a larger vertical stress applied to the wall.

The loads applied during the first phase did not determine any damage in the wall. Consequently, no initial stiffness reduction was observed at the beginning of the second phase of the test.

The first four cycles of the test showed an elastic behaviour. First flexural horizontal cracks appeared along the first top and bottom head joints at the bottom left corner during cycle 5, and then at the other corners of the wall in cycle 6. During cycle 11, new cracks diagonally oriented opened, along the mortar joint. The evolution at the top of the wall is shown in Figure 21a,b and Figure 22a for the top and the bottom portion of the wall, respectively. At end stage, crushing of the toes and sliding can also be observed (Figure 23a,b). The failure mode was mainly governed by flexure.

The lateral displacements required the introduction of a torque at the top of the wall (provided by the axial forces applied by the vertical actuators, as explained in equation (3) of section 1.3) in order to maintain the top and bottom of the sample parallel; large displacements can therefore induce compressive forces in the actuators. The test was stopped at a net drift of 1,3%, when compressive loads in one of the two pairs of actuators caused the instability of the loading system (the actuators are double hinged and apply the load by pulling). The instability determined a severe damage of the top portion of the wall; consequently, the test was stopped before than an effective failure of the wall, so that no reduction of the lateral shear resistance was observed.

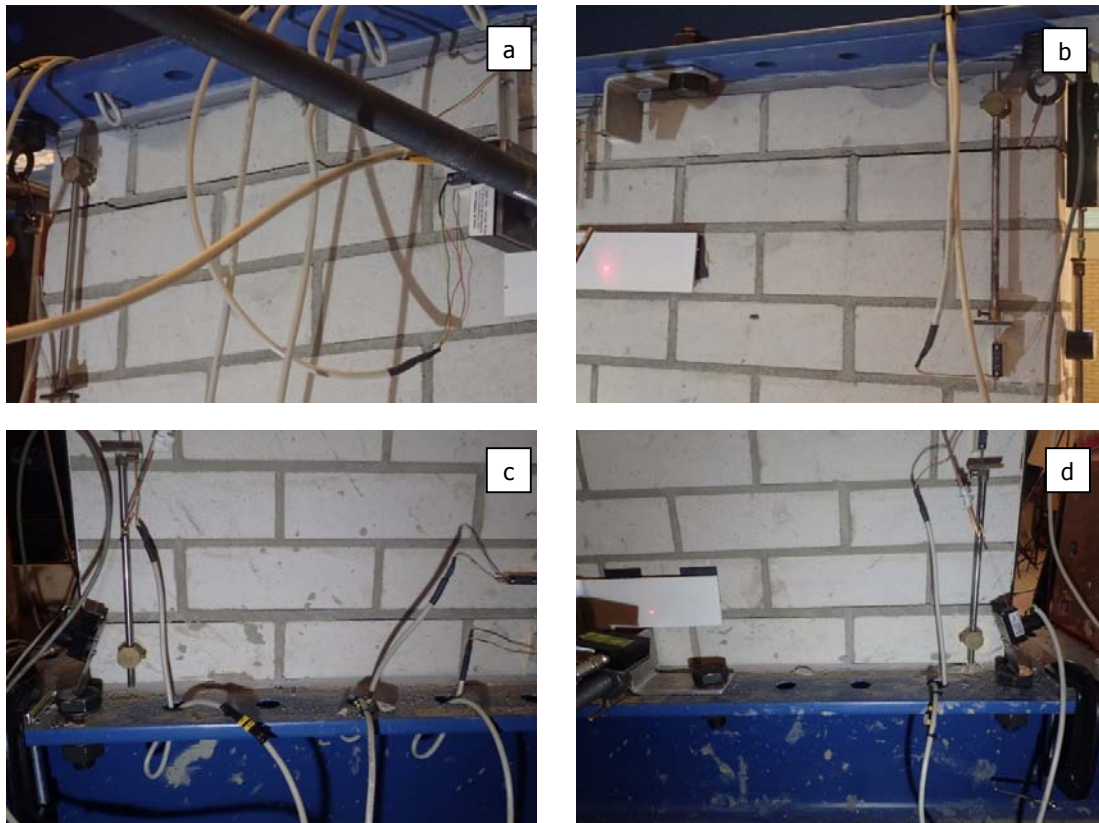


Figure 21. TUD_COMP-3: Rocking cracks at the bottom and top ends of the wall: details of the left (a) and right (b) top toes (cycle 9), and of the left (c) and right (d) bottom toes (cycle 8).

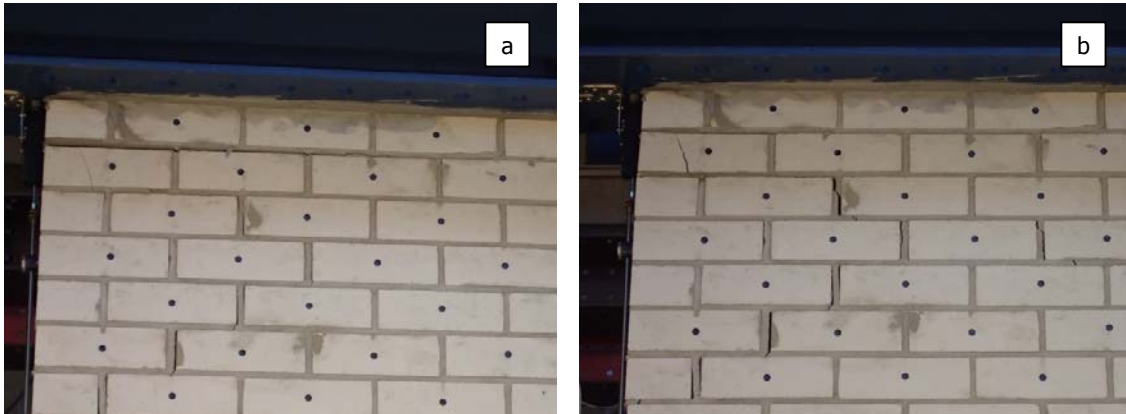


Figure 22. TUD_COMP-3: Evolution of the crack pattern in the top portion of the wall for positive drifts: cycle 10 (horizontal crack along the bed joint - a) and cycle 11 (diagonal cracks - b).

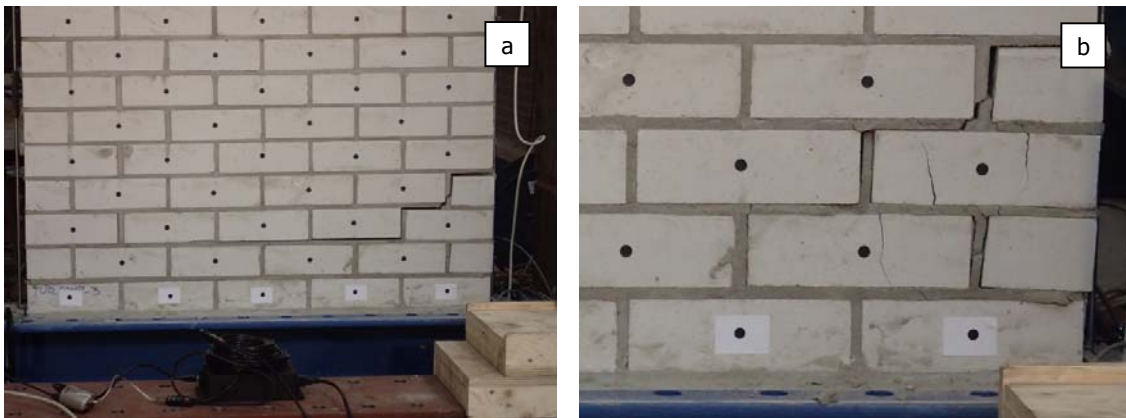


Figure 23. TUD_COMP-3: Crack pattern at end stage: details of the bottom portion of the wall for negative loading (a) and toe crushing (b).

3.5 TUD_COMP-4

The recorded net drifts of the wall measured at the positive and negative extremes of each cycle are listed in Table 9.

Table 9. Adopted loading scheme for sample TUD_COMP-4.

Cycle	Measured net drift (%)		Measured net amplitude (mm)	
	Positive displacements	Negative displacements	Positive displacements	Negative displacements
1	0,003	-0,003	0,09	-0,09
2	0,006	-0,006	0,18	-0,18
3	0,01	-0,01	0,27	-0,27
4	0,013	-0,013	0,36	-0,35
5	0,018	-0,018	0,51	-0,49
6	0,037	-0,037	1,03	-1,03
7	0,057	-0,057	1,57	-1,57
8	0,1	-0,1	2,66	-2,66
9	0,2	-0,2	5,39	-5,35

During a pre-test to determine the stiffness of the top frame, a horizontal crack was formed in between the first and second bricklayer from the top, caused by the unloading of the actuators. The crack was repaired by gluing steel plates on both sides of the wall, making a stiff connection between the first and second top bricklayers. The consequence is that during the test, cracking of the bed joints is possible below the second bricklayer, instead of below the first layer; de facto the specimen was one bricklayer shorter. The described restoration is shown in Figure 24.



Figure 24. Detail of the repaired top bricklayer of TUD_COMP-4.

The behaviour of the specimen under the imposed cyclic loading can be described as follow. The first four cycles of the test showed an elastic behaviour. The secant stiffness increases until cycle 3 and after that cycle decreases; indeed, for small forces the stiffness is lower than for large (Figure 25a). Since the nonlinearities can be observed in the recordings of the forces (measured by the load cell of the horizontal actuator – 19 in Figure 4 and Table 2), whereas the net displacements of the wall are perfectly linear (Figure 25), the change of stiffness is probably due to some play in the test frame which could not be identified and removed; for this reason, the same issue occurs during all the three tests on the long walls (TUD_COMP-4/6). However, this behaviour should not be visible in numerical simulations, and the initial stiffness of the wall should be slightly higher than the value derived from cycle 3 (223 kN/mm). The first visible cracks (four diagonal cracks from the corners, connected by a short horizontal crack in the middle of the panel) were visible in cycle 6; the cracks started to develop close to the centre of the panel (Figure 27a), and quickly expanded to the corners (Figure 27b). At the end of the test (Figure 27) the horizontal crack width was much larger than the maximum imposed displacement, clearly showing the presence of residual sliding. Indeed, in the last cycles, the top part of the wall moved over the middle bed joint over three bricks, causing the crushing of the mortar (Figure 28a); that movement allowed the top part of the wall to clamp the loose side triangles, move them further outwards, and, eventually, leave them in that position (and move them again the next step). The test was stopped when the loose triangles were close to be sheared out of the top and bottom part, as shown in Figure 28b.

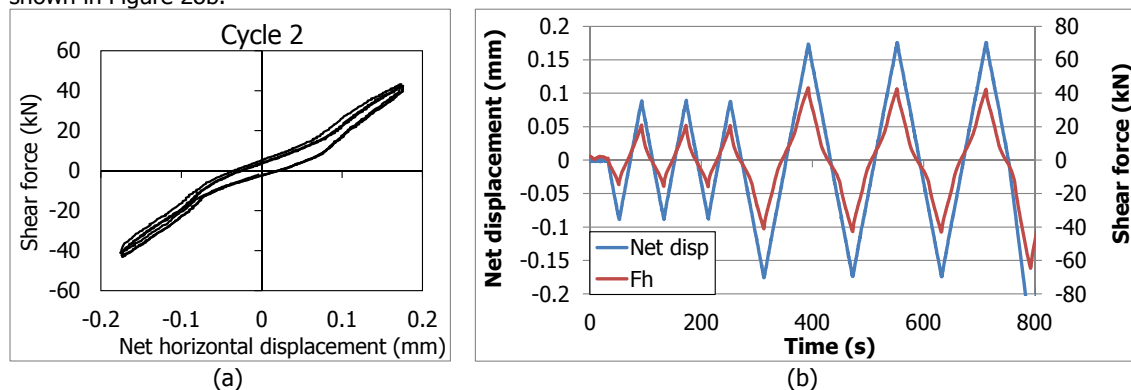


Figure 25. Initial cycles of sample TUD_COMP-4: details of the nonlinearities of the recorded forces in the elastic domain.

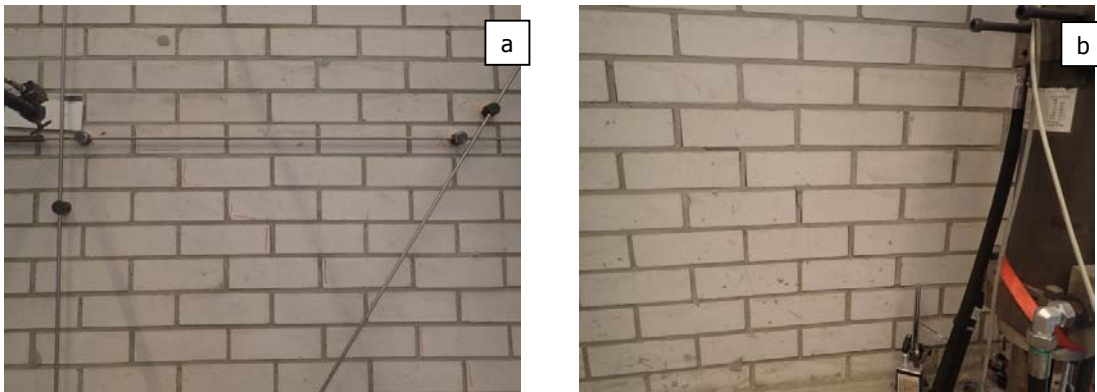


Figure 26. TUD_COMP-4: Diagonal cracks in the middle of the panel (a) and close to the corners (b).

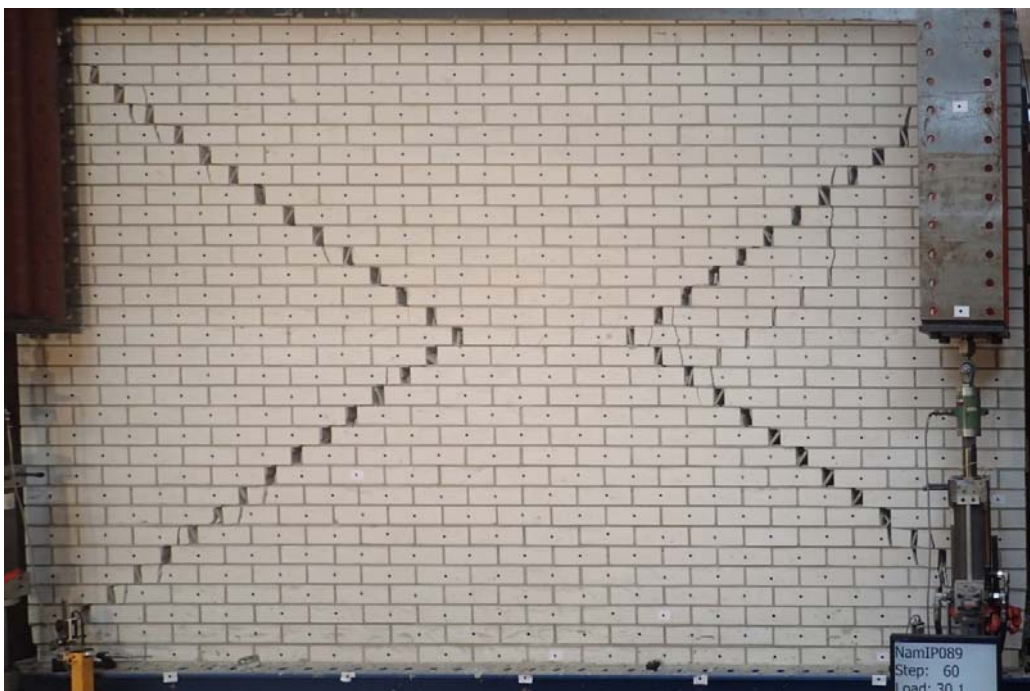


Figure 27. TUD_COMP-4: Crack pattern at end stage.

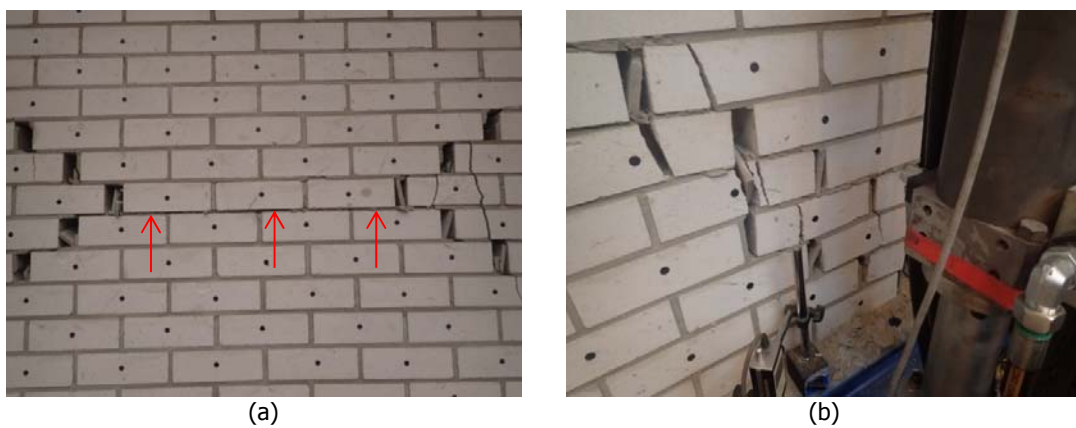


Figure 28. TUD_COMP-4: details of the crack pattern at end stage. Crushing of the mortar bed joint at the centre of the wall (a); shearing out of the loose triangle at the bottom corner (b).

3.6 TUD_COMP-5

The recorded net drifts of the wall measured at the positive and negative extremes of each cycle are listed in Table 10.

Table 10. Adopted loading scheme for sample TUD_COMP-5.

Cycle	Measured net drift (%)		Measured net amplitude (mm)	
	Positive displacements	Negative displacements	Positive displacements	Negative displacements
1	0.003	-0.002	0,07	-0,05
2	0.005	-0.005	0,13	-0,13
3	0.007	-0.007	0,20	-0,20
4	0.01	-0.01	0,27	-0,28
5	0.02	-0.02	0,40	-0,40
6	0.05	-0.06	1,46	-1,51
7	0.09	-0.10	2.53	-2.72
8	0.08	-0.18	2.1	-5.0
9	-0.15	-0.39	-4.1	-10.7
10	-0.34	-0.46	-9.5	-12.7

Similarly to specimen TUD_COMP-4, during the placing of the beams on the top of the wall, a horizontal crack developed in between the first and the second bricklayer from the top; however, the crack was not continuous for the whole length of the joint, and was localised in the central part of the specimen. The crack was then repaired by gluing steel plates on both sides of the wall, making a stiff connection between the first and second top bricklayers, as shown in Figure 29. Therefore, in the same way of specimen TUD_COMP-4, the cracking of the bed joints could occur below the second bricklayer, instead of below the first layer; de facto the specimen was one bricklayer shorter.



Figure 29. Detail of the repaired top bricklayer of TUD_COMP-5.

Similarly to specimen TUD_COMP-4 and for same reasons, the secant stiffness increases until cycle 3 and after that cycle decreases.

The first visible cracks were observed during cycle 6, given by a combination of a diagonal crack and a horizontal crack along the mortar joint between the first and the second bricklayer from the bottom; the crack intercepted not only the mortar joints, but also some bricks (Figure 30).

At increasing imposed amplitudes, other minor cracks opened; however, at end of the test, the main crack trace the pattern of the first crack (Figure 31 and Figure 32a). A vertical crack close to the edge of the wall crosses the brick and the mortar layers (Figure 32b).

Similarly to specimen TUD_COMP-4, at the end of the test the horizontal width of the main cracks was much larger than the maximum imposed top displacement. This is caused by the residual sliding which could be observed at the left-bottom corner of the wall (Figure 32c).

After the peak load, the asymmetric damage of the wall (the bottom-right corner was more severely damaged than the opposite one) determined a redistribution of the forces in the actuators in order to guarantee zero rotations (hence a clamped condition) at the top of the wall. Because of this, the force in the right actuators (actuators 1 and 2) decreased gradually cycle after cycle for the same imposed displacement, reaching negative values (of traction), as displayed in Figure 33. For this reason in cycles 8

and 9 the displacements could be increased in one direction only (i.e. negative direction), and not go back to zero. It should be noted that compression stresses acted on the top of the wall during the whole test, because the forces of traction in the actuators were compensated by the self-weight of the steel structure on the top of the wall.

The test had to be stopped because the asymmetry in the loads of the vertical actuators did not allow anymore to reverse the imposed displacement.

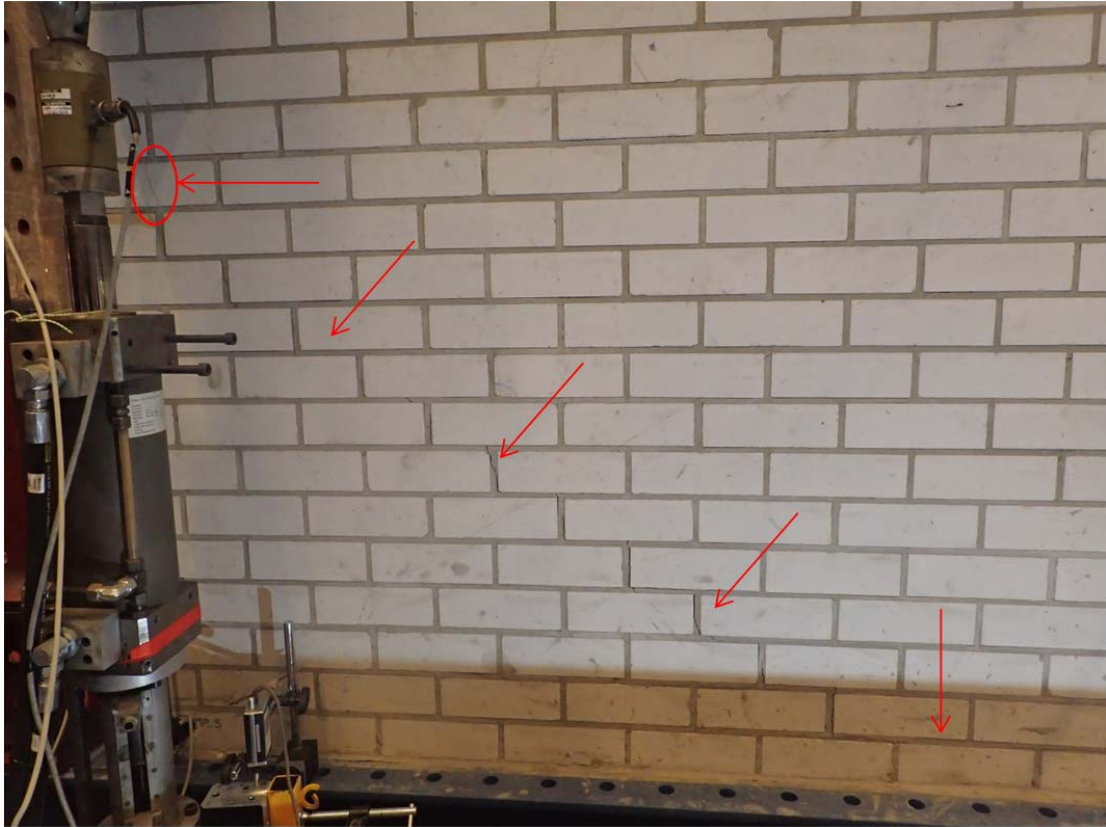


Figure 30. TUD_COMP-5: first cracks during cycle 6.



Figure 31. TUD_COMP-5: crack pattern at end stage.

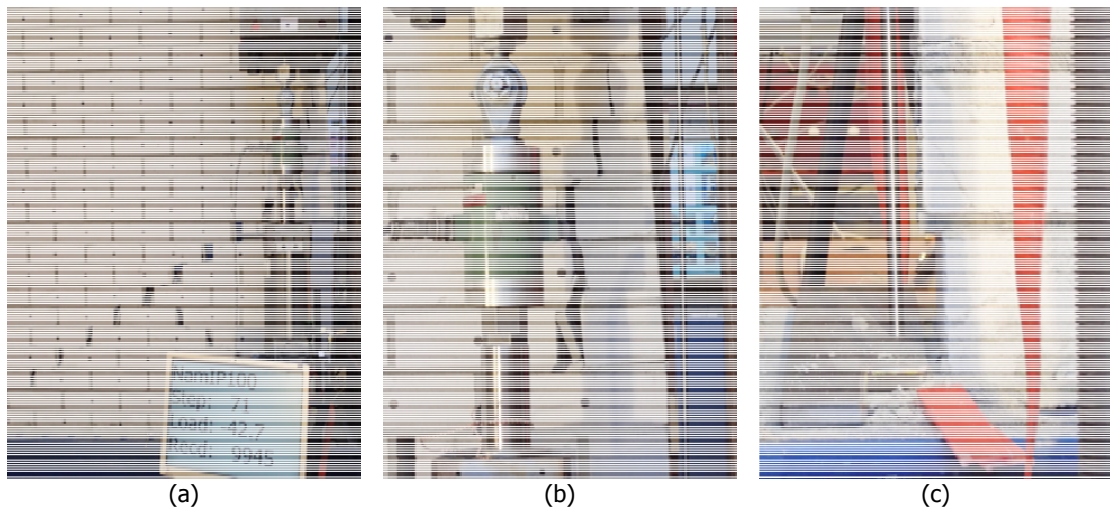


Figure 32. TUD_COMP-5: details of the crack pattern at the end of the test. Diagonal cracks at the bottom-right corner of the wall (a); vertical crack across the bricks (b); residual sliding at the bottom left corner (c).

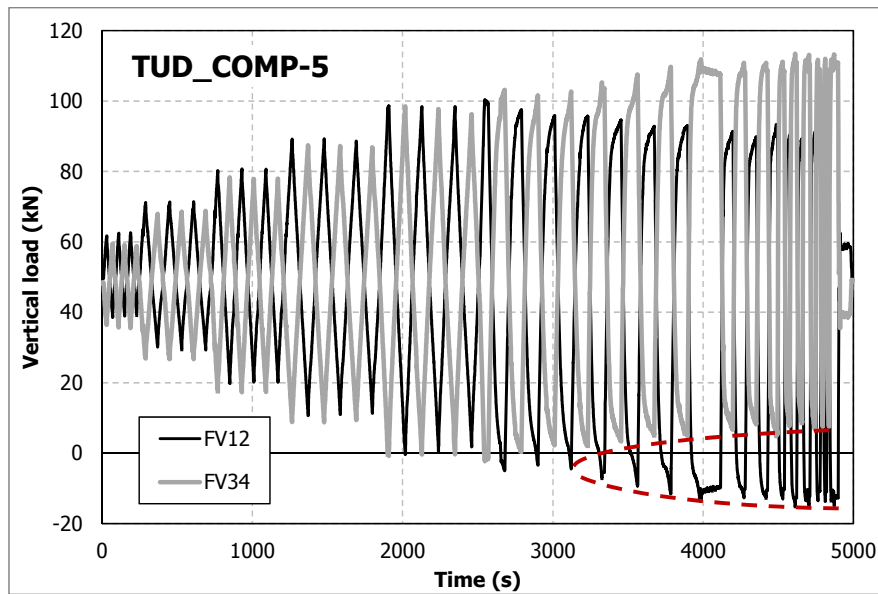


Figure 33. TUD_COMP-5: vertical force applied by the left (FV34) and right (FV12) actuators to the specimen during the test.

3.7 TUD_COMP-6

The recorded net drifts of the wall measured at the positive and negative extremes of each cycle are listed in Table 11.

Table 11. Adopted loading scheme for sample TUD_COMP-5.

Cycle	Measured net drift (%)		Measured net amplitude (mm)	
	Positive displacements	Negative displacements	Positive displacements	Negative displacements
1	0.004	-0.004	0.11	-0.11
2	0.007	-0.007	0.21	-0.21
3	0.011	-0.011	0.31	-0.31
4	0.015	-0.015	0.41	-0.42
5	0.021	-0.021	0.57	-0.58
6	0.042	-0.045	1.15	-1.24
7	0.080	-0.085	2.20	-2.34
8	0.16	-0.17	4.38	-4.54
9	0.36	-0.37	9.93	-10.1
10	0.46	-0.47	12.7	-12.8
11	0.56	-0.56	15.4	-0.11

The first four cycles showed an elastic behaviour. However, similarly to specimen TUD_COMP-4 and TUD_COMP-5 some play in the test frame determined a reduction of stiffness around zero forces; for this reason, the secant stiffness increased slightly after cycle 1, remained almost stable until cycle 4 and after that cycle decreased.

The first visible cracks were observed during cycle 5, along the main diagonal of the wall (Figure 34a). This gave horizontal deformations that were detected by the transducer measuring the horizontal deformation at mid-height over the length of the wall (Figure 35), and the crack intercepted not only the mortar joints, but also some bricks (Figure 34c).

At increasing imposed amplitudes (cycles 6-9), the diagonal cracks got larger and larger, more than one crack opened along the diagonal for negative loading, the bottom corners started to be pushed off the wall and residual sliding appeared (Figure 37).

The brick crushing in the central portion of the panel and at corners caused after cycle 9 a significant reduction of resistance of the wall; a reduction of 36% and 39% at the end of the test for positive and negative displacements, respectively was measured.

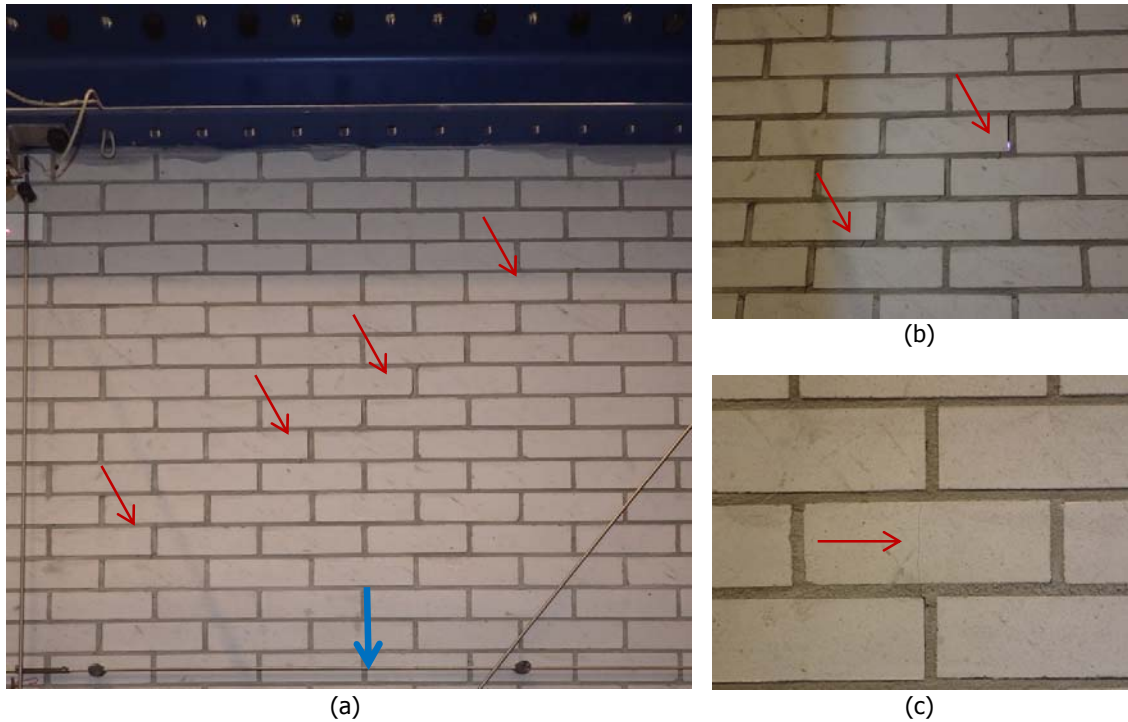


Figure 34. First cracks visible in cycle 5. General overview (a) and details (b,c). The blue arrow points out the horizontal measuring device, for which the results are plotted in Figure 35.

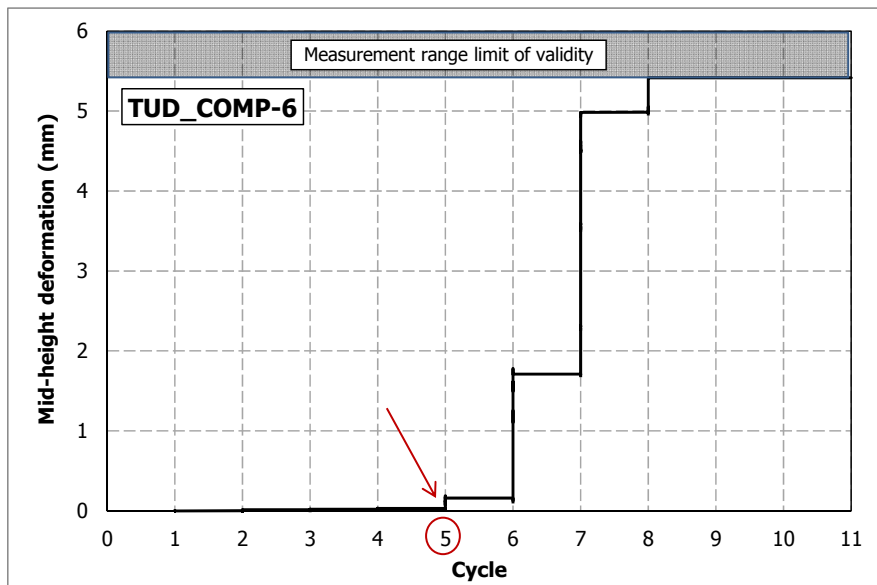


Figure 35. TUD_COMP-6: Mid-height horizontal deformation of the wall vs Loading cycle. See also Figure 34.

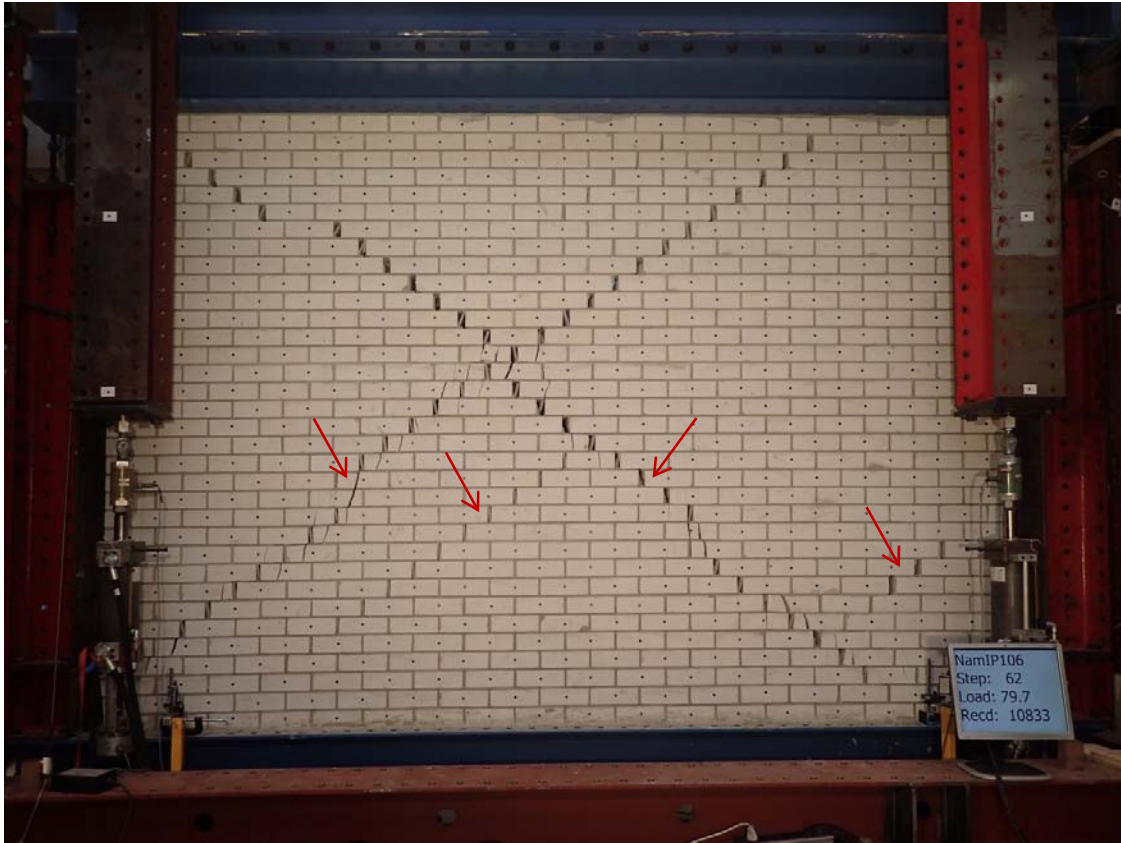


Figure 36. Cracks visible at the end of cycle 9.

At the end of the test the detected crack pattern (Figure 37) is similar to that described at the end of cycle 9; however, more diagonal cracks appeared also for positive loading. Besides, the crack width is larger and the crushing along the diagonals, and especially in the central region of the panel (Figure 38a) and at corners (Figure 38b), is more evident.

Similarly to specimen TUD_COMP-4 and TUD_COMP-5, at the end of the test the width of the main cracks was much larger than the largest displacement imposed to the wall. This was caused by the residual sliding along the cracks.

The test was stopped because the corners were eventually supported by the steel columns of the loading frame, so that any further result would have been affected by these accidental supports (Figure 39). Besides, the imposition of larger displacements could determine the collapse of the damaged toes, compromising the stability of a portion or of the whole wall, and causing its collapse.

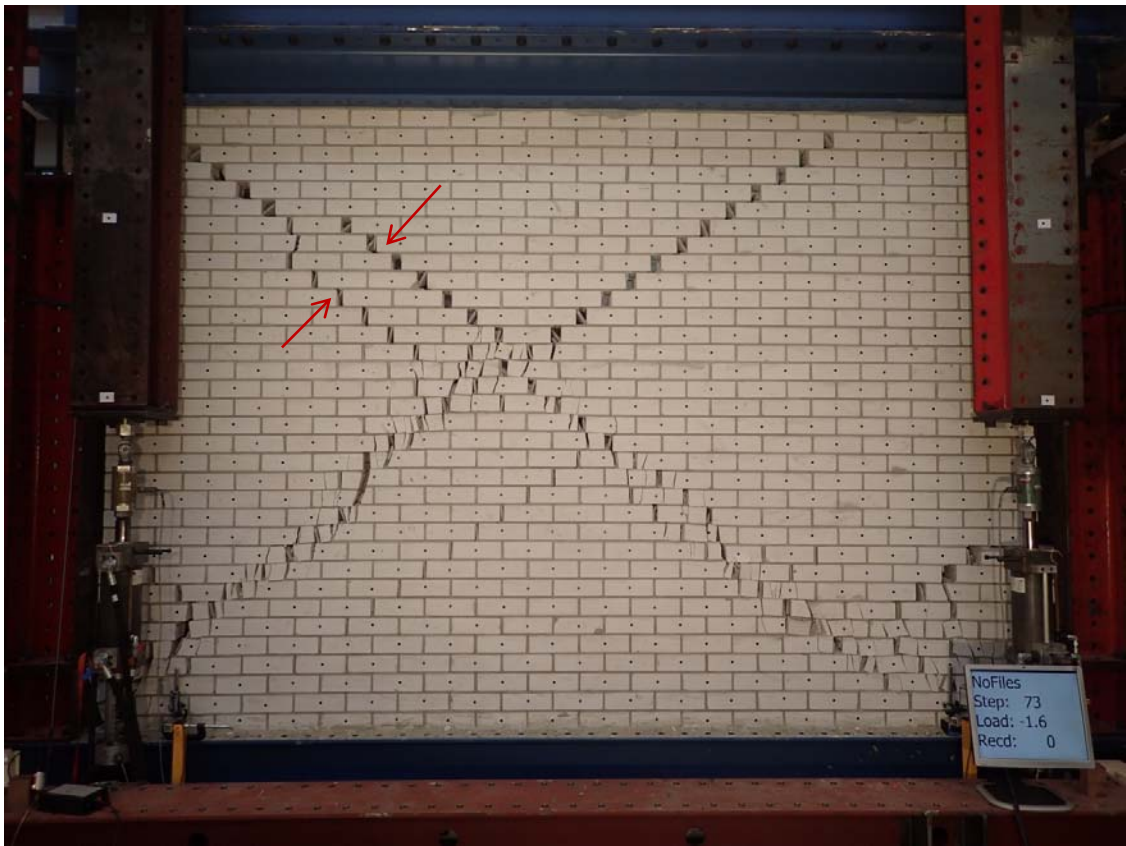


Figure 37. TUD_COMP-6: crack pattern at end stage.

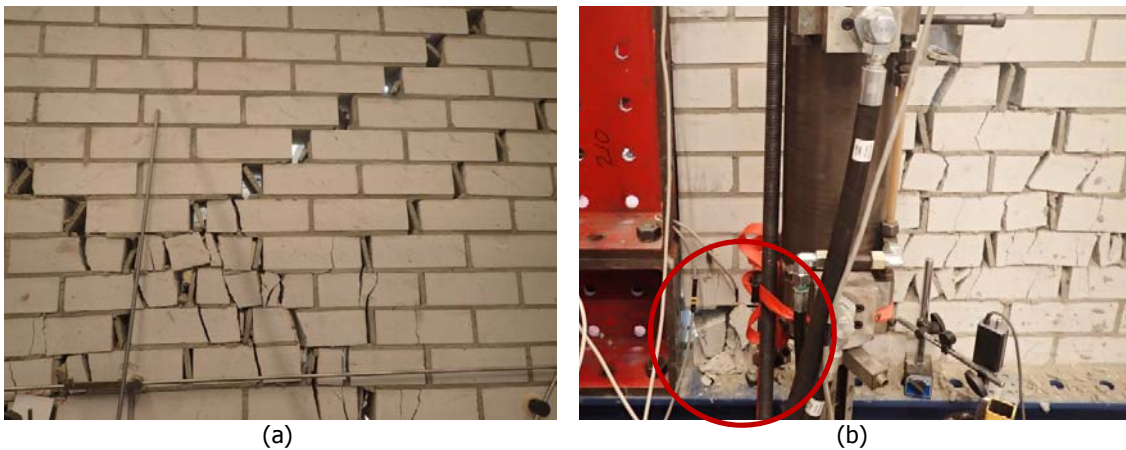


Figure 38. TUD_COMP-6: detail of the crushing of bricks in the central portion (a) and at the bottom-right corner (b) of the wall at the end of the test.

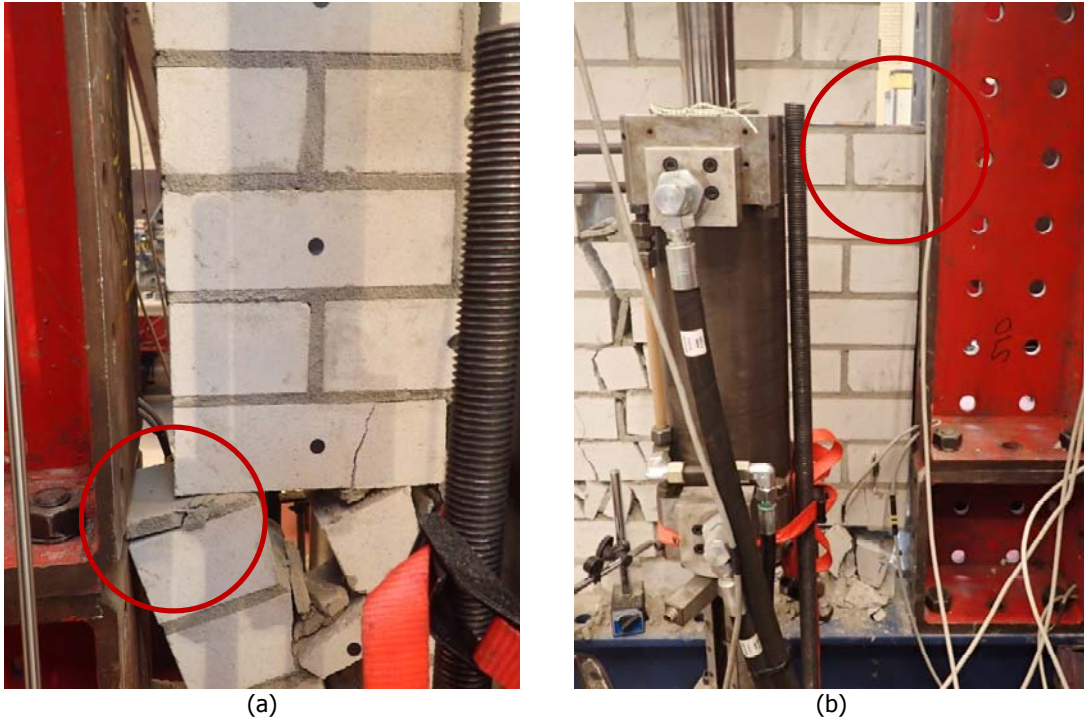


Figure 39. TUD_COMP-6: detail of the left (a) and right (b) corners supported by the steel columns at the end of the test.

4 Comparison with values proposed by the codes

The resistance if the tested samples could be estimated in accordance with the equations provided by the Eurocode 8 [1] for the assessment of existing masonry buildings. Specifically, according to the code, the shear capacity of an unreinforced masonry wall can be controlled by either flexure or shear.

The shear force capacity of an unreinforced masonry wall as controlled by flexure under an axial load P , may be taken according to equation (C.1) of section 4.2.1(3) in [1]:

$$V_f = \frac{LP}{2H_0} \left(1 - 1.15 \frac{\sigma_v}{f'_m} \right) \quad (6)$$

where L is the in-plane horizontal dimension of the wall (depth), H_0 is the distance between the section where the flexural capacity is attained and the contraflexure point ($H_0=H$ for cantilever walls, and $H_0=0.5H$ for double clamped walls), $\sigma_v=P/(Lt)$ is the applied vertical pressure, t is the wall thickness, and f'_m is the mean compressive strength of the masonry.

The shear force capacity of an unreinforced masonry wall controlled by shear under an axial load P , may be taken according to equation (C.2) of section 4.3.1(3) in [1]:

$$V_s = f_{vd} L' t \quad (7)$$

where:

- L' is the depth of the compressed area of the wall;
- t is the wall thickness;
- f_{vd} is the masonry mean shear strength accounting for the presence of vertical load.

Similarly to the formulation suggested in the code, f_{vd} is evaluated according to a frictional law (based on a Mohr-Coulomb formulation, which can be physically justified especially in the cases where diagonal cracking is associated with mortar bed- and head-joint failure), according to the following equation:

$$f_{vd} = f_{v0} + \mu \sigma_v \quad (8)$$

being f_{v0} the initial shear strength of the material (i.e. the mean shear strength in absence of vertical load), μ the friction coefficient (whereas in equation (C.2) μ is substituted by the constant value 0.4), and $\sigma_v=P/(Lt)$ is the applied vertical pressure.

However, the equation reported in the code does not provide a direct evaluation of L' . An explicit prediction of the shear strength, where a calculation of the compressed length of the wall L' is included, is provided in [2], and can be computed according to the following equation:

$$V_s = Lt \left(\frac{1.5f_{v0} + \mu \sigma_v}{1 + 3 \frac{H_0}{L} \cdot \frac{f_{v0}}{\sigma_v}} \right) \quad (9)$$

The capacity of an unreinforced masonry wall is evaluated as the smallest between the values given by equations (6) and (9):

$$V = \min(V_f; V_s) \quad (10)$$

The predicted resistance and failure mode, evaluated according to equations (6), and (10) for each test is reported in Table 12.

In Table 12 are listed the properties which vary for each test. Geometric and material properties which do not change are the following:

- the height ($H=2760$ mm) and the thickness ($t=102$ mm) of the walls;

- the mean compressive strength of the calcium silicate masonry ($f'_m = 5.93$ MPa), as reported in [3];
- the initial shear strength of the calcium silicate masonry ($f_{v0} = 0.14$ MPa), as reported in [3];
- the shear friction coefficient of the calcium silicate masonry ($\mu = 0.43$), as reported in [3].

All the obtained experimental results are in line with the predictions, unless the specimen TUD_COMP-2, for which a significantly lower resistance is obtained.

A comparison between the predicted resistance and failure mode, and the experimental results for each test is reported in Table 13.

Table 12. Calculated shear resistance and failure mode of the tested specimens.

Sample name	L	σ_v	H/H_0	V_f	V_s	V	Failure mode
	mm	MPa	-	kN	kN	kN	
TUD_COMP-0a	1100	0.7	0.5	27.1	32.7	27.1	Flexure
TUD_COMP-1	1100	0.7	1	13.5	22.9	13.5	Flexure
TUD_COMP-2	1100	0.5	1	10.1	15.3	10.1	Flexure
TUD_COMP-3	1100	0.4	0.5	16.5	18.5	16.5	Flexure
TUD_COMP-4	4000	0.5	0.5	267	134	134	Shear
TUD_COMP-5	4000	0.3	0.5	167	93	93	Shear
TUD_COMP-6	4000	0.5	1	134	110	110	Shear

Where D = depth of the wall; σ_v = vertical pressure; H/H_0 = shear ratio; V_f , V_s = predicted shear strength for flexure and shear failure, respectively; V = predicted shear strength.

Table 13. Shear resistance and failure mode of the tested specimens: comparison between the experimental and the predicted results.

Sample name	Experimental			Predicted	
	V^+	V^-	Failure mode	V	Failure mode
	kN	kN		kN	
TUD_COMP-0a	27.7	-30.6	Flexure/Shear	27.1	Flexure
TUD_COMP-1	9.9	-9.1	Flexure/Shear	13.5	Flexure
TUD_COMP-2	9.4	-9.6	Flexure/Shear	10.1	Flexure
TUD_COMP-3	15.0	-14.2	Flexure/Shear	16.5	Flexure
TUD_COMP-4	119	-123	Shear	134	Shear
TUD_COMP-5	102	-103	Shear	93	Shear
TUD_COMP-6	110	-109	Shear	110	Shear

Where V^+ , V^- = experimental shear strength for positive and negative displacements, respectively; V = predicted shear strength.

5 Conclusions

In the Stevin 2 laboratory of the Delft University of Technology replicated calcium silica walls have been cyclically under in-plane loading conditions.

On overview of the test results is given in Table 14.

Table 14. Overview on the main results from the performed in-plane tests.

Specimen	Dimensions	BC	σ_v	K_{in}	V^+	V^-	$d_{r,f}$	Prevailing failure mode
	L(m) x H (m) x t (m)		(MPa)	(kN/mm)	(kN)	(kN)	(%)	
TUD_COMP-0a	1.1 x 2.76 x 0.102	DC	0.7	25.8	27.7	-30.6	0.9	Combined: - Flexure; - Toe crushing; - Sliding.
TUD_COMP-1	1.1 x 2.76 x 0.102	C	0.7	7.2	9.94	-9.11	0.9	Combined: - Flexure; - Toe crushing; - Sliding.
TUD_COMP-2	1.1 x 2.76 x 0.102	C	0.5	7.7	9.40	-9.57	1.6	Combined: - Flexure; - Sliding.
TUD_COMP-3	1.1 x 2.76 x 0.102	DC	0.4	22.4	15.0	-14.2	1.3	Combined: - Flexure; - Toe crushing; - Sliding.
TUD_COMP-4	4.0 x 2.76 x 0.102	DC	0.5	223	119	-123	0.2	Shear diagonal cracks along joints.
TUD_COMP-5	4.0 x 2.76 x 0.102	DC	0.3	288	102	-103	0.45	Sliding along the bottom mortar joint.
TUD_COMP-6	4.0 x 2.76 x 0.102	C	0.5	125	110	-109	0.55	Shear diagonal cracks along joints and toe crushing.

Where BC = boundary conditions; σ_v = vertical pressure; K_{in} = initial stiffness (measured as the secant stiffness between the extreme displacements of each cycle); V^+ , V^- = shear strength for positive and negative displacements, respectively; $d_{r,f}$ = final drift (drift at which the test was stopped); DC = double clamped wall; C = cantilever wall.

The following points can be addressed:

- The measured shear values are in line with predicted values according to the codes and literature, except for TUD_COMP-1, whose resistance is lower than the predicted value.
- The observed stiffnesses of the walls are consistent with the properties derived in the companion material tests [3].
- The prevailing failure mode depends mainly on the shear ratio H/L (in the considered cases by the wall length): combined flexure and sliding for the short specimens and shear failures for the long specimens.
- The reported final drifts are the drifts at which the test was stopped, not the ultimate drift capacity of the walls. In most cases the final drift was determined by limitations in the set-up (as detailed explained in section 3), rather than by the effective failure of the specimens
For future experiments the test set-ups can be adjusted to enable larger drifts in the test.

- Especially for the short walls, the flexural cracks did not start at the extreme (top/bottom) mortar rows as expected, but a few brick layers above. A repetition of this test configuration with a different masonry typology in a future test program might be useful to investigate if this phenomenon is a property of this specific type of masonry or is related to the test set-up.
- Especially for the long specimens, the head joints openings at the end of the test were extremely larger than the horizontal displacements imposed at the top of the wall.

References

- [1] EN 1998-3+C1 (2013). Eurocode 8 – Design of structures for earthquake resistance - Part 3: Assessment and retrofitting of buildings. Nederlands Normalisatie-instituut (NEN).
- [2] Magenes, G., and Calvi, G. M., (1997). In-plane seismic response of brick masonry walls. *Earthquake engineering & structural dynamics*, 26(11), 1091-1112.
- [3] University of Technology of Delft (2015). Tests for the characterization of replicated masonry (v07).